Citation: Moradi, S., Khaksar, T., Nazarinia, A., Hussain, A., 2022. Petrology and geochemistry of Plio-Quaternary high-Nb basalts from Shahr-e-Babak area: Insights into post-collision magmatic. Geologica Acta, 20.8, 1-19.
DOI: 10.1344/GeologicaActa2022.20.8

geologica acta

Petrology and geochemistry of Plio-Quaternary high-Nb basalts from Shahr-e-Babak area: Insights into post-collision magmatic processes in the Kerman Cenozoic Magmatic Arc

S. Moradi[1] T. Khaksar[1] A. Nazarinia[2] A. Hussain[3]

[1]Department of Geology, Tarbiat Modares University
Tehran, Jalal Al Ahmad, 14115-175, Iran

[2]Department of Geology, Faculty of Sciences, University of Hormozgan
Bandar Abbas, Iran

[3]State Key Laboratory of Geological Processes and Mineral Resources, Collaborative Innovation Center for Exploration of Strategic Mineral Resources, School of Earth Resources, China University of Geosciences
Wuhan 430074, PR China

ABSTRACT

Post-collision Pliocene-Quaternary basaltic rocks outcrop in the Kerman Cenozoic Magmatic Arc (KCMA) to the northwest and east of Shahr-e-Babak city. These porphyritic and vesicular basaltic rocks are composed essentially of clinopyroxene, olivine, and plagioclase. These basalts display alkaline affinity and negative Ta, Zr, Rb anomaly, but slightly negative Nb anomaly, relative to elements with similar compatibility, and positive Ba, K, Sr anomaly, suggesting their magma source related to subduction-accretion with implication of subducted slab derived components to the source. In the primitive mantle and chondrite normalized diagrams, these rocks show trace elements (except depletion in Nb, Ta) and Rare Earth Element (REE) patterns similar to the Ocean Island Basalts (OIB) and share trace and major element characteristics similar to High-Nb Basalts (HNBs). Geochemical analyses for major and trace elements suggest that the Shahr-e-Babak HNBs have undergone insignificant crustal contamination and minor olivine + Fe-Ti oxide ±clinopyroxene fractional crystallization. These HNBs derived from a partial melting (~5%) of garnet-peridotite mantle wedge, which have already metasomatized by overlying sediments, fluids, and adakitic (slab-derived) melts as major metasomatic agents in post-collision setting in the KCMA. We conclude that asthenospheric upwelling arising from slab break-off followed by the roll-back of subducting Neotethys slab also triggered metasomatized peridotite mantle wedge and caused its partial melting in the subduction zone.

KEYWORDS **High-Nb basalts. Post-collision. Metasomatized mantle wedge. Slab break-off. Kerman Cenozoic Magmatic Arc.**

INTRODUCTION

Cenozoic magmatic rocks are well exposed in the Iranian Plate, in the north of the Bitlis-Zagros Suture Zone (Fig. 1), which resulted from steep and oblique subduction of Neo-tethyan oceanic lithosphere under the Cental Iranian Micro-continental Block (CIMB) and Anatolian blocks during Late Mesozoic, Cenozoic and its subsequent collision of Arabian plate with Eurasia (Agard *et al*., 2011; Dercourt *et al*., 1986; Mouthereau *et al*., 2012; Stampfli and Borel., 2002).

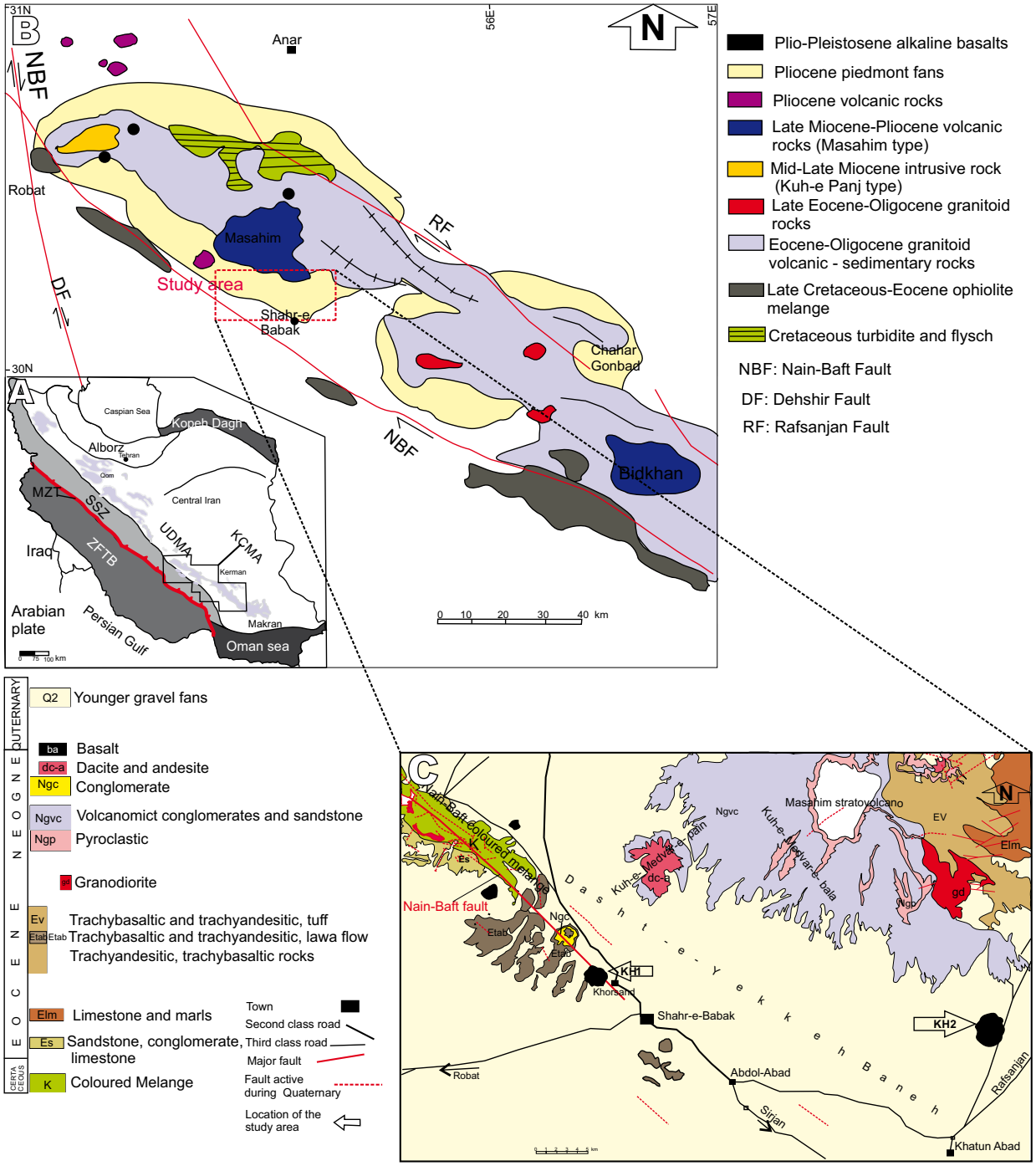

FIGURE 1. A) Simplified geotectonic map of Iran; B) Simplified geological map of Kerman Cenozoic Magmatic Arc (Dimitrijevic, 1973; Stocklin and Nabavi, 1973) showing location of study area; C) Simplified geological map of the study area, northwest and east of Shahr-e-Babak (modified from Geological map of Iran, 1:100000 Sardic *et al.*, 1971).

The diversity of post-collision alkaline to sub-alkaline volcanism and plutonism, recently considered as result of partial melting of lithospheric mantle modified and metasomatized during subduction of the Neo-Tethyan oceanic slab (s) have occurred in the Urumieh-Dokhtar Magmatic Arc (UDMA) a part of the eastern Turkish, Armenian, and Iranian Zagros orogenic plateaus (Allen *et al.*, 2013; Azizi *et al.*, 2014; Kheirkhah *et al.*, 2013; Neill *et al.*, 2015; Özdemir *et al.*, 2006; Saadat and Stern, 2012). This type of magmatism is usually characterized by within-plate and/or subduction-related geochemical features (Pearce *et al.*, 1990, 2003).

The Pliocene-Quaternary magmatism in the southern part of the UDMA contains adakitic rocks and the High-Nb Basalts (HNBs) show alkaline affinity. The HNBs are characterized by unusual High-Field Strength Elements (HFSEs), high Nb content (>18ppm), and low Large-Ion Lithophile Elements/ (LILE)/HFSE and Heavy Rare Earth Elements/Light Rare Earth Elements (HREE/LREE) ratios (*e.g.* Azizi *et al.*, 2014; Castillo *et al.*, 2007; Mazhari, 2016). They also show high, TiO_2 and P_2O_5 content,, high values of Sr/Y (>25) and La/Yb (>14) ratios, and low Rb/Sr ratio, and Yb content (Castillo, 2008; Hastie *et al.*, 2011).

The study of post-collisional magmatic mafic rocks especially HNBs provides a unique opportunity to identify the asthenospheric-lithospheric properties (Carlson *et al.*, 2005), geodynamic processes, and tectonic settings (*e.g.* Castillo, 2012; Dilek and Furnes, 2011). The tectonic and magma evolution of the UDMA has been studied widely (*e.g.* Khaksar *et al.*, 2020; Moradi *et al.*, 2021; Nazarnia *et al.*, 2018). However, very few investigations on the petrology and geochemistry of the alkaline basalts and HNBs, with or without associated adakites, have been published. The aim of this study is to review the petrographical and chemical composition of the Shahr-e-Babak HNBs, in the Kerman Cenozoic Magmatic Arc (KCMA), in order to provide new constraints on the conditions of their genesis and source region. The study herein suggests a tectono-magmatic model to explain the evolution of the post-subduction arc magmatism in the Shahr-e-Babak area.

GEOLOGICAL SETTING

Urumieh-Dokhtar Magmatic Arc

The Zagros Orogenic Belt (ZOB), in the central part of the Alpine-Himalayan orogenic belt, generated as a result of the NE-dipping subduction of the Neo-Tethys oceanic lithosphere, accretion and subsequent collision of the Arabian plate with the CIMB (*e.g.* Alavi, 1994; Berberian and King, 1981). The Zagros Fold and Thrust Belt (ZFTB) (Berberian and King, 1981; Mohajjel and Fergusson, 2000), the Sanandaj-Sirjan Zone (SSZ), and the UDMA are the three major sub-parallel tectono-stratigraphic structures in the ZOB (Fig. 1).

The SSZ is separated from the ZFTB to the southwest and from the UDMA to the northeast by the main Zagros thrust fault and fore-arc depressions respectively (Alavi,1994; Glennie, 2000).

The UDMA is considered to be an active continental margin (Moin Vaziri, 1991; Takin, 1972; Verdel *et al.*, 2011) about 1000km long, 50km wide and 4km thick (Berberian and Berberian, 1981), extending from NW to SE in central Iran. The magmatism in the UDMA is generally composed of subduction-related voluminous calc-alkaline, and locally tholeiitic rocks (*e.g.* Azizi and Jahangiri, 2008; Omrani *et al.*, 2008) from Cretaceous to Quaternary age. However, the peak of magmatic activity is thought to have been in the Eocene with a notable magmatic flare-up from ~55Ma to ~37Ma (Verdel *et al.*, 2011).

The younger volcanic activity in the UDMA was mainly alkaline (Amidi *et al.*, 1984; Moradian, 1997) and associated with post-collisional tectono-magmatic processes (Richards, 2003). The timing of collision is controversial, some authors suggested it was before or during the late Miocene (*e.g.* Allen *et al.*, 2004; Mohajjel *et al.* 2003,) while other, (Hassanzadeh,1993), proposed the late Miocene and/or the late Neogene. According to Berberian and King (1981) and Jahangiri (2007), the onset of the alkaline volcanic activity in the UDMA (6-5 Ma) was due to the sinking of the final broken pieces of oceanic slab to a depth where alkaline melts were generated.

The distinctive southeastern part of the UDMA is known as the Dehaj-Sarduiyeh volcano-sedimentary belt (Dimitrijevic, 1973) or KCMA (Fig. 1A). The KCMA is about 450km long and 80km wide (Dewey *et al.*, 1973) and mainly composed of calc-alkaline volcano-plutonic rocks (Zarasvandi *et al.*, 2007). It host porphyry copper deposits, several of them of large size and many of small–medium size (Taghipour, 2007; Zarasvandi *et al.*, 2011). The volcanic and plutonic activities in the KCMA are considered to have reached their peaks in the middle Eocene and Oligocene-Miocene, respectively (Hassanzadeh, 1993).

Shahr-e-Babak region

The two investigated zones are situated in the KCMA, between the Rafsanjan and Nain-Baft faults (Nain-Baft ophiolite belt), more precisely, at 8km to the northwest (KH1, near to Khorsand village) and at 22km to the east (KH2, near to Khatoon Abad village) of Shahr-e-Babak city in the southern slope of the Masahim volcano, (Fig. 1B, C). The magmatism in this area is represented by Paleogene basaltic andesites, latites, tephrites, nepheline phonoliths, and volcano-clastic rocks (Ghadami *et al.*, 2008; Hosseni *et al.*, 2009). Oligocene-Miocene granodiorites, porphyric diorites and porphyric quartz diorites, Miocene-Pliocene adakites (Ghadami *et al.*, 2008; Ghadami, 2009) and Pliocene-Quaternary alkaline volcanic rocks (Amidi *et al.*, 1984; Hosseni *et al.*, 2009).

Almost fifty Plio-Pleistocene granitoid, dacitic to rhyodacitic subvolcanic domes occur in the Eocene-Oligocene volcanic and volcano-sedimentary rocks in Shar-e-Babak area (Dimitrijevic *et al.*, 1971, Ghadami *et al.*, 2008).

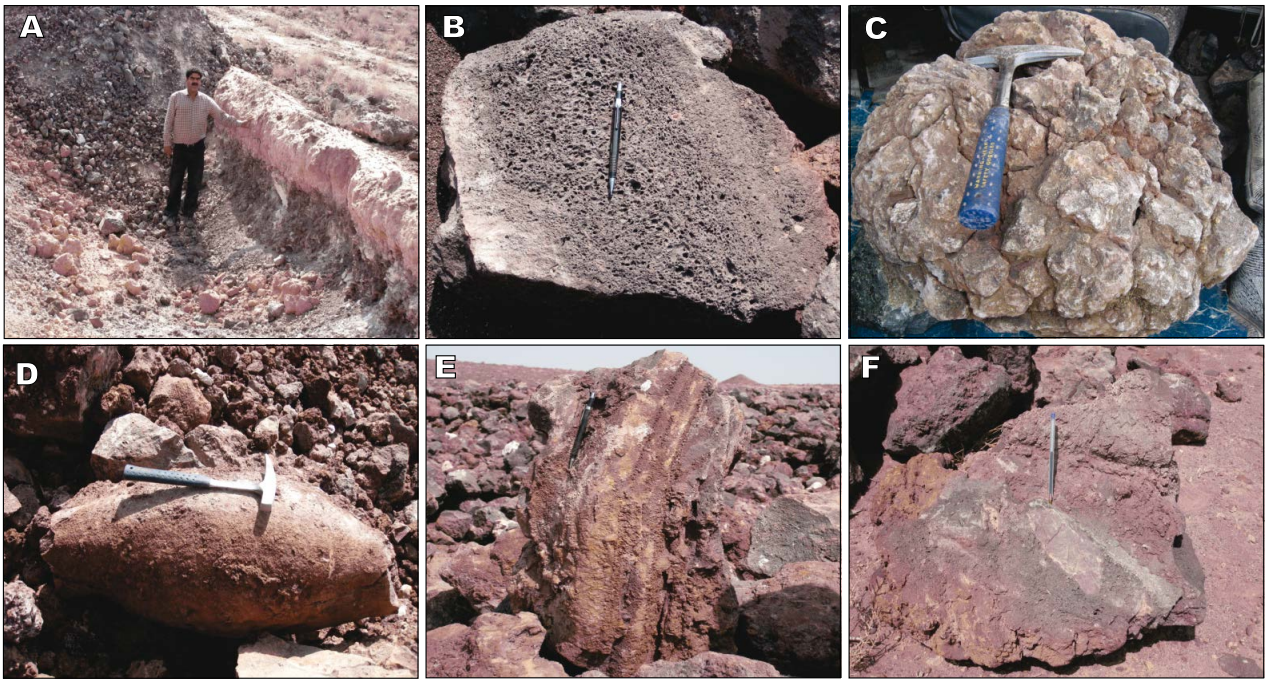

FIGURE 2. A) View of basaltic rocks covered by Quaternary sediments; B) Vesicular basaltic rock from Shahr-e-Babak; C) Bread-crust bomb; D) Spindle shaped bomb; E) Toothpaste shaped bomb; F) Basaltic rock with fragments of older rocks.

The contemporaneous eruption of mafic alkaline melts is a conspicuous feature in the Shahr-e-Babak area (Berberian and King, 1981). Pleistocene monogenetic basalts and trachy basalts occur in the Chah-Bagh, Takhte-Siah, Khatoon Abad, and Khorsand localities, whereas the basaltic trachyandesite occurs in the localities of Chah-Breshk and Tale-Ghorban (Hosseni *et al.*, 2009).

There are also a series of northeast–southwest-trending faults, with small inferred displacements, developed in shear zone associated with the Nain-Baft and Rasanjan faults (Fig. 1A) that likely have controlled ascent and emplacement of magmas and ore-deposit formation in the Shahr-e- Babak area.

As a whole, it seems that the Tertiary volcanic rocks in Shahr-e-Babak area formed during three stages: i) an explosive volcanic event including pyroclastic material (ash and spinel bombs), ii) an efusive basaltic lava distributed around cones and vesicular basaltic rocks (scoria) and iii) an explosive event with vesicular basaltic rocks and bombs erupted in the final stage of the volcanism.

FIELD DESCRIPTIONS AND PETROGRAPHY

The Plio-Quaternary volcanism in Shahr-e-Babak area is represented by small basaltic scoria cones and lava flows. These volcanic rocks are exposed in two areas, where they overlie unconformably Neogene volcanic rocks (Saric and Djordjevic, 1971) and are usually covered by thick layers of Quaternary sediments (Fig. 2A). They include vesicular basaltic rocks, lapilli, tuff, volcanic bombs and basaltic lavas.

The Shahr-e-Babak basaltic rocks are generally highly porphyritic. They show vesicular texture and are dark gray or brown to black colour with a red leaching patch, that most probably formed due to the presence of iron oxides/hydroxide phases during evolution of these rocks (Fig. 2B). Different types of volcanic bombs are seen in the studied area, *e.g.* bread-crust bombs, cylindric bombs, cannonball bombs, spindle bombs, pear and toothpaste shaped bombs (Fig. 2C-E,). Bombs show relatively low porosity (~20%) as compared with other basaltic rocks, and sometimes include partly epidotized fragments from the Naein-Baft ophiolite mélange and particles of rock that are probably from the cryptodome intruded immediately before the volcanic eruption (Fig. 2F). The Shahr-e-Babak basaltic rocks have been classified as olivine basalt and tracky basalt. Porphyry texture is the dominant texture of these rocks, though glomeroporphyry and sieve textures in plagioclase and, rarely, in clinopyroxene are also observed (Fig. 3A, B, D). The basalts are composed of phenocrysts of olivine, clinopyroxene and, rarely, plagioclase, and titano-magnetite as accessory mineral (Fig. 3A) embedded in glassy to fine-grained groundmass consisting of microlitic

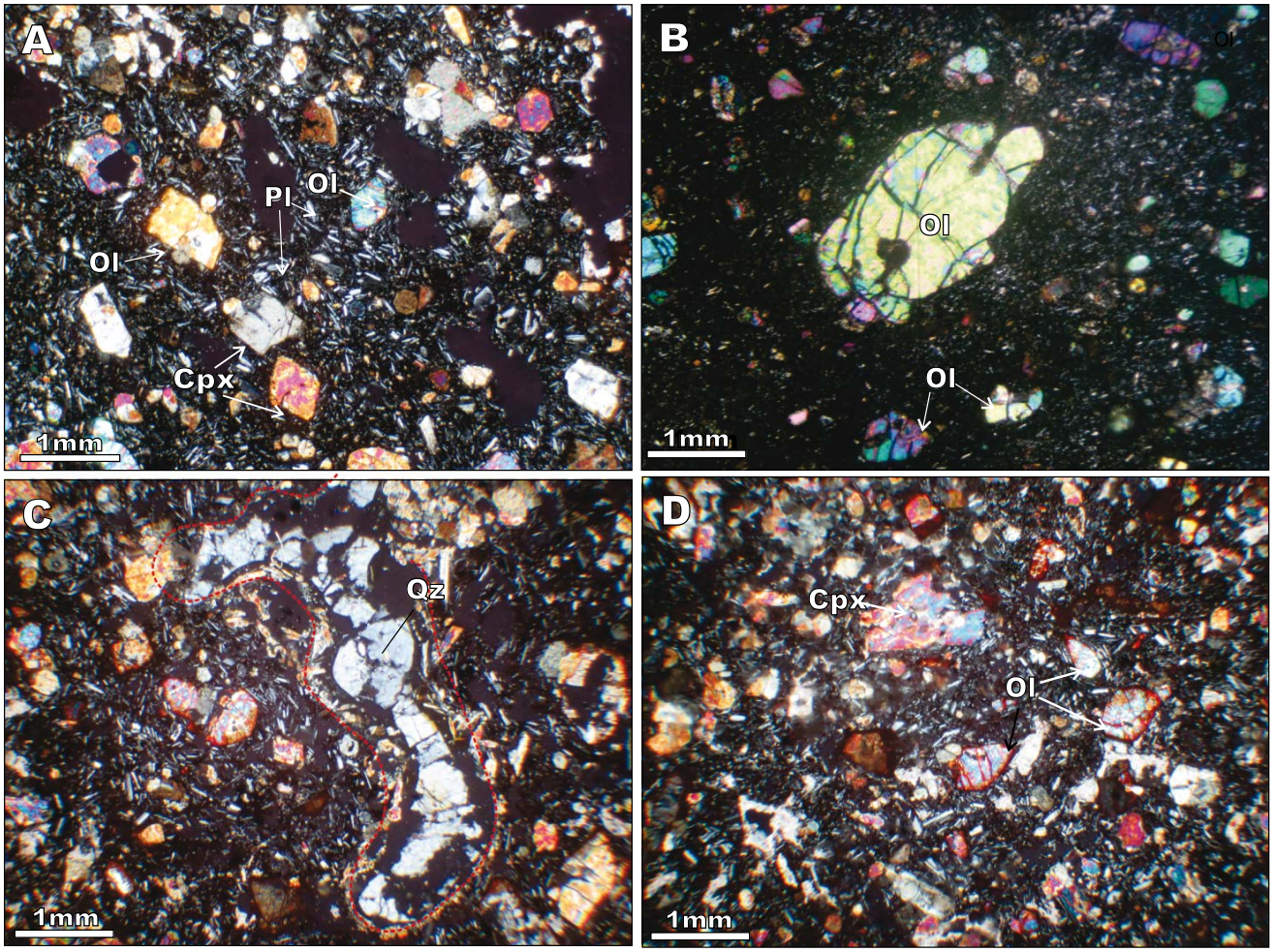

FIGURE 3. A) Clinopyroxene and olivine phenocrysts in a porphyric basalt; B) Olivine phenocryst with absorbed margins in a basaltic rock; C) Amygdaloidal basalt; D) Clinopyroxene and idingisitized olivine phenocrysts. Abbreviation from Whitney and Evans (2010): Pl= Plagioclase; Ol= Olivine; Cpx= Clinopyroxene; Qz= Quartz.

plagioclase, small olivine, clinopyroxene, and opaque minerals with amygdaloidal texture, rarely filled by calcite and quartz (Fig. 3C). The vesicles show primary porosity of the rocks which are generated via degassing during lava extrusion (Navarro *et al*., 2020).

Olivine phenocrysts are homogeneously distributed in the groundmass; however, in some places, they form glomeroporphyry texture along with clinopyroxen minerals. They are subhedral to euhedral, mostly fresh but some are altered to iddingsite along the margins and cracks (Fig. 3D). Clinopyroxene phenocrysts (augite) are the second most abundant mafic mineral in these basaltic rocks. They are mostly euhedral, some subhedral, up to 1-5mm long, and fresh. The plagioclase is confined to the groundmass with length <0.5mm as small laths, fresh and show albite and Carlsbad twinning with weakly to strongly develop trachytic texture (Fig. 3A).

ANALYTICAL METHOD

Based on microscopic observations, we selected 15 samples of basalt for whole-rock chemical analysis to be performed in the analytical laboratories of the SGS Minerals, Toronto, Canada. Major oxide abundances were determined by X-Ray Fluorescence (XRF) and recalculated to 100%, volatile free (Table 1). Approximately a 50g split of each sample was pulverized to fine powder in an agate ring mill. The powdered samples were dried at 75–90°C to eliminate adsorbed water, ignited at 950±50ºC and then fused with 50% lithium metaborate ($LiBO_2$) and 50% lithium tetraborate ($Li_2B_4O_7$) in a fluxer to produce a glass disc. The glass disc was analyzed on the sequential XRF spectrometer. Quantitative determination was made through previously prepared calibration standards. Data reduction was done using laboratory information management system software that performs all necessary calculations automatically to calculate the percent oxide for

TABLE 1. Major and trace elements in the studied rocks

	KH1							KH2							
Sample	Sm-26	Sm-02	Sm-06	Sm-10	Sm-15	Sm-16	Sm-19	Tm-03	Tm-06	Tm-16	Tm-23	Tm-24	Km-03	Km-05	Km-06
Major elements (wt%)															
SiO_2	49.0	48.9	47.8	49.5	48.3	48.3	49.4	45.4	47.4	48.5	46.7	47.2	46.3	48.9	46.6
TiO_2	1.3	1.3	1.3	1.3	1.2	1.3	1.3	1.2	1.2	1.3	1.2	1.3	1.1	1.3	1.4
Al_2O_3	14.0	14.0	13.6	13.8	13.5	13.8	13.9	14.0	13.7	14.0	13.8	14.1	13.2	13.7	12.9
FeO_t	9.1	8.9	8.9	9.2	9.2	9.2	9.3	8.6	9.0	9.1	8.9	9.2	9.1	9.2	9.6
MnO	0.2	0.2	0.2	0.2	0.2	0.2	0.1	0.2	0.2	0.2	0.2	0.2	0.2	0.2	0.2
MgO	10.3	9.9	8.0	9.4	10.1	10.0	10.4	8.5	8.9	8.8	6.7	8.0	8.8	9.8	9.7
CaO	9.2	9.9	11.4	9.7	9.7	9.6	9.9	11.4	10.0	9.9	11.1	10.6	12.4	9.8	11.5
Na_2O	3.4	3.2	3.5	3.6	3.4	3.1	3.6	2.7	2.8	3.3	2.7	3.3	2.7	3.4	4.1
K_2O	1.8	1.7	2.0	1.9	1.8	2.0	1.6	1.9	1.8	2.3	2.8	2.5	2.1	1.9	1.6
P_2O_5	0.5	0.5	0.5	0.5	0.5	0.5	0.5	0.5	0.6	0.6	0.6	0.6	0.5	0.5	0.7
LOI	0.9	2.0	2.6	1.0	1.3	1.2	0.8	4.0	2.8	1.7	3.4	2.5	2.9	1.4	2.0
Mg#	66.8	66.4	61.6	64.7	66.2	65.9	66.7	63.7	63.6	63.1	57.1	60.9	63.2	65.4	64.3
K_2O/Na_2O	0.5	0.5	0.6	0.5	0.5	0.6	0.4	0.7	0.6	0.7	1.0	0.8	0.8	0.6	0.4
Trace elements (ppm)															
V	238.0	245.0	227.0	247.0	239.0	249.0	249.0	274.0	259.0	265.0	330.0	261.0	210.0	237.0	269.0
Co	46.0	46.4	43.1	45.3	46.6	44.8	46.1	41.9	41.8	40.6	39.9	40.2	42.1	43.8	43.4
Ni	240.0	236.0	195.0	205.0	244.0	201.0	225.0	170.0	172.0	168.0	157.0	155.0	176.0	197.0	117.0
Zn	79.0	79.0	85.0	87.0	81.0	89.0	86.0	90.0	93.0	95.0	95.0	94.0	90.0	82.0	91.0
Cu	72.0	69.0	71.0	52.0	79.0	71.0	55.0	112.0	122.0	54.0	27.0	146.0	64.0	66.0	107.0
Ga	16.0	16.0	16.0	17.0	16.0	16.0	17.0	17.0	17.0	17.0	17.0	17.0	15.0	16.0	16.0
Rb	36.8	28.6	40.1	38.2	40.2	41.0	14.8	45.2	32.1	26.8	52.1	62.4	40.0	41.2	45.1
Sr	710.0	880.0	770.0	960.0	670.0	840.0	760.0	1010.0	1030.0	1420.0	4420.0	1020.0	760.0	1420.0	1020.0
Y	18.2	18.1	17.9	18.6	17.7	18.6	18.2	17.3	17.4	17.2	16.9	17.1	16.4	18.8	17.7
Zr	108.0	109.0	104.0	109.0	104.0	108.0	107.0	109.0	110.0	108.0	107.0	109.0	90.7	111.0	106.0
Nb	20.0	30.0	20.0	30.0	20.0	30.0	30.0	20.0	20.0	20.0	20.0	20.0	20.0	20.0	30.0
Mo	<2	<2	<2	<2	<2	<2	<2	<2	<2	<2	<2	<2	<2	<2	<2
Sn	1.0	1.0	<1	1.0	<1	<1	<1	1.0	<1	<1	1.0	3.0	<1	<1	3.0
Cs	0.7	0.5	0.7	0.7	0.8	0.7	0.9	0.8	0.8	1.1	0.7	1.1	0.8	0.8	1.4
Ba	700	690	760	730	690	770	900	1350	2180	1390	1360	1360	920	720	1350
La	28.3	28.3	27.4	28.7	28.3	30.2	28.6	31.2	31.1	30.5	31.1	31.4	27.4	28.3	39.0
Ce	56.5	57.3	55.6	58.4	58.0	60.3	57.9	65.9	66.6	65.8	65.8	66.4	57.3	57.1	83.8
Pr	6.8	6.9	6.6	7.0	7.0	7.2	7.0	8.1	8.2	8.1	8.2	8.2	7.0	6.9	10.3
Nd	26.7	27.0	25.7	27.1	26.9	27.7	27.1	32.4	32.9	32.2	32.1	32.1	28.1	26.9	39.2
Sm	5.0	5.0	4.7	5.2	5.0	5.1	4.8	5.9	5.9	5.9	5.9	5.9	5.0	5.1	6.7
Eu	1.5	1.6	1.4	1.5	1.5	1.5	1.5	1.6	1.6	1.6	1.6	1.6	1.4	1.5	1.7
Gd	4.0	4.5	4.3	4.4	4.2	4.4	4.1	4.5	4.5	4.7	4.3	4.5	4.0	4.5	4.8
Tb	0.6	0.6	0.6	0.6	0.6	0.6	0.7	0.6	0.7	0.7	0.6	0.6	0.5	0.6	0.7
Dy	3.6	3.9	3.7	3.9	3.8	3.7	3.8	3.8	3.8	3.5	3.6	3.7	3.3	3.8	3.7
Ho	0.8	0.7	0.8	0.8	0.8	0.8	0.7	0.7	0.7	0.7	0.7	0.7	0.7	0.7	0.7
Er	2.0	2.1	2.0	2.2	2.0	2.3	2.0	1.9	2.0	1.9	1.9	1.9	1.7	2.1	1.9
Tm	0.3	0.3	0.3	0.3	0.3	0.3	0.3	0.3	0.3	0.3	0.3	0.3	0.3	0.3	0.3
Yb	1.8	1.7	1.9	2.0	1.7	1.9	1.8	1.6	1.7	1.7	1.6	1.7	1.7	1.8	1.7
Lu	0.3	0.3	0.3	0.3	0.2	0.3	0.3	0.2	0.3	0.2	0.3	0.2	0.2	0.3	0.3
Hf	3.0	3.0	3.0	3.0	3.0	3.0	3.0	3.0	3.0	3.0	3.0	3.0	3.0	3.0	3.0
Ta	0.9	0.9	0.9	0.9	0.9	0.9	0.9	0.5	0.6	0.6	0.6	0.6	0.6	1.0	1.0
W	<1	<1	<1	<1	<1	<1	<1	<1	<1	<1	<1	<1	<1	<1	<1
Tl	<0.5	<0.5	<0.5	<0.5	<0.5	<0.5	<0.5	<0.5	<0.5	<0.5	<0.5	<0.5	<0.5	<0.5	<0.5
Th	4.0	3.9	3.8	4.0	3.9	4.2	4.0	3.9	4.0	4.0	4.1	4.2	3.6	4.0	5.2
U	1.0	0.9	1.0	0.9	1.0	1.0	1.0	1.0	0.7	1.2	1.3	1.3	0.8	1.0	1.1
Eu/Eu*	1.02	1	0.98	0.98	1	0.99	1.03	0.94	0.94	0.95	1	0.92	0.93	0.96	0.9
Sum_REE	138.24	140.15	135.22	142.35	140.31	146.18	140.63	158.65	160.09	157.84	158.06	159.24	138.63	139.91	194.73

each element and the percent total major-element content of the sample, including Loss On Ignition (LOI). The detection limit was 0.01wt% of the oxide.

Trace elements of the bulk rock were analyzed with Inductively Coupled Plasma–Mass Spectrometry (ICP-MS). Approximately 0.1g of powdered rock samples were fused by Na-peroxide in graphite crucibles and dissolved using dilute HNO_3. The fused solution was aspirated into the ICP-MS where the ions were measured and quantified according to their unique mass. The used detection limit was vary during analysis for different elements. It was 5ppm for Cu, Ni, V; 2ppm for Mo; 1ppm for Ag, Ga, Hf, Nb, Sn, W; 0.5ppm for Co, Ta, Tl, Y, Zr; 0.2ppm for Rb; 0.1ppm for Ce, Cs, La, Nd, Sm, Th, Yb and 0.05ppm for Dy, Eu, Er, Gd, Ho, Lu, Pr, Tb, Tm.

RESULTS

Whole-rock geochemistry

The major and trace element concentrations in the samples are presented in Table 1. Whole-rock SiO_2 content

of these basaltic samples ranges between 45.4 and 49.5wt%, with high Na_2O+K_2O content (~4.6–5.8wt%). All samples have MgO>6.7wt% with Mg number from 57.1 to 66.8. The LOI values are 0.9 to 3.4wt%, except in one sample with 4wt% (Table 1). These rocks are classified as basalt and trachybasalt in the SiO_2 versus total alkali (Na_2O+K_2O) diagram (Fig. 4A). In the Zr/Ti versus Nb/Y diagram (Fig. 4B), the studied samples plot in the alkali basalt field. The samples plot in the alkaline series in the SiO_2 versus K_2O diagram (Fig. 4C) and slightly fall within the transition field between potassic and sodic series in the Na_2O versus K_2O diagram (Fig. 4D).

Primitive mantle normalized (Sun and McDonough, 1989) spider diagram of trace-element abundances for the Plio-Quaternary basalts in the studied area show that these rocks are enriched in LILEs compare to HFSEs (Fig. 5B). Most of the samples show positive Sr, K, Ba anomaly and negative Zr, Rb, and Ta, but slightly negative Nb anomaly. The studied basaltic rocks are considered as HNB with Nb concentration from 20 to 30ppm.

The plot of REE normalized by chondrite (Sun and McDonough, 1989; Fig. 5A) shows an enrichment of LREE than HREEs for the Shahr-e-Babak HNBs with La/Yb_{CN}= 9.7-13 and around 100 to 200 times chondrite for the LREE and about 10-20 times chondrite for the HREE.

The REE content in these samples is high, ranging from 135.2 to 194.7ppm (average= 150ppm). The average values of Eu*/Eu and Ce/Ce* are 0.97 and ~1, respectively, which basically do not show a Eu anomaly. All samples show similar trends, suggesting similar REE fractionation degrees and magma source. They are well correlated with Ocean Island Basalt (OIB) (Fig. 5A) and are distinct from Enriched Mid Oceanic Ridge Basalt

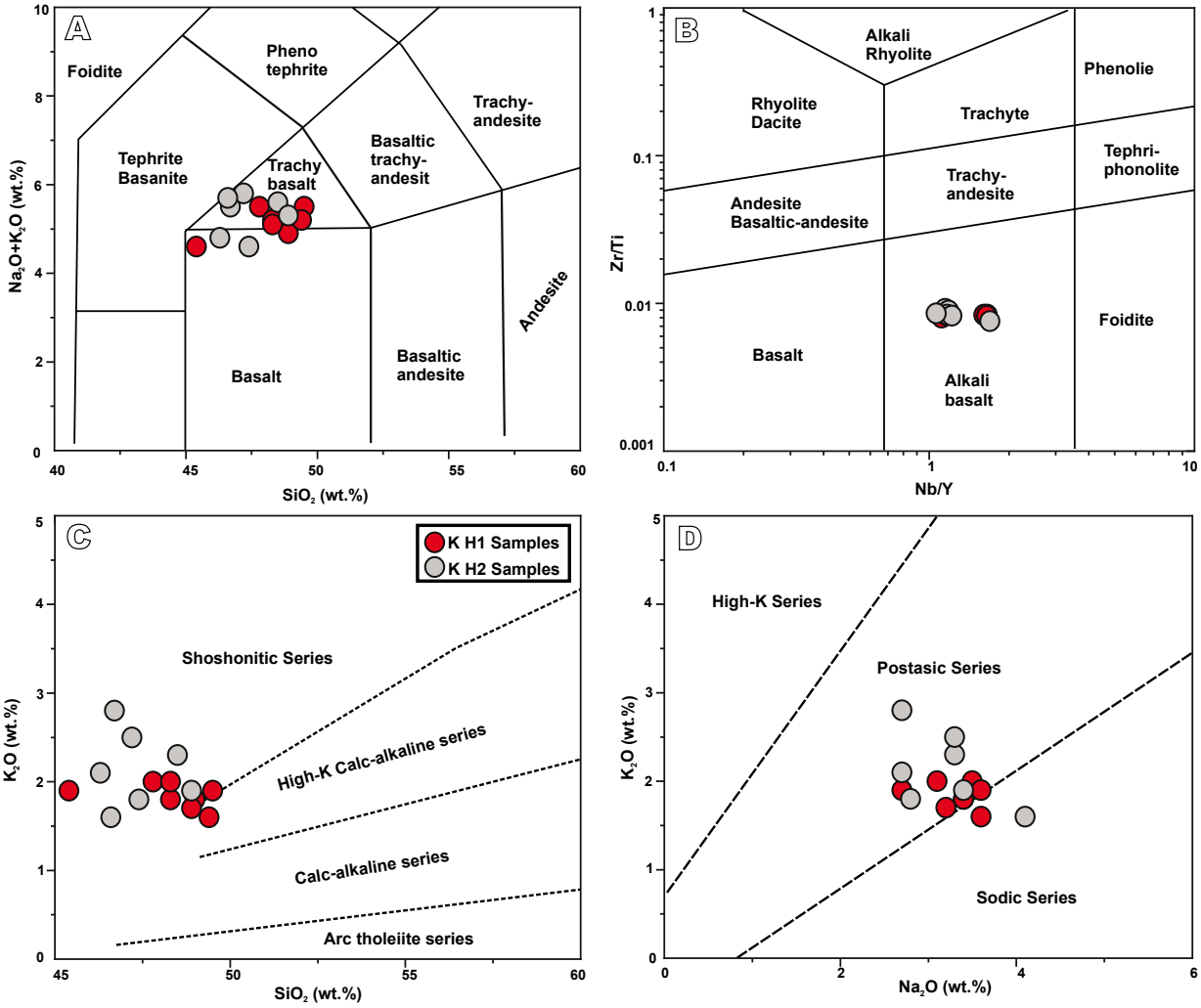

FIGURE 4. A) Total Alkali versus Silica (TAS) diagram (LeBas *et al.*, 1986); B) Nb/Y versus Zr/Ti classification diagram (Winchester and Floyd, 1977); C) SiO_2 versus K_2O diagram from Peccerillo and Taylor (1976); D) Na_2O versus K_2O diagram (Le Maitre, 2002). The red circle is sample from KH1 area and the gray circle is sample from KH2 area.

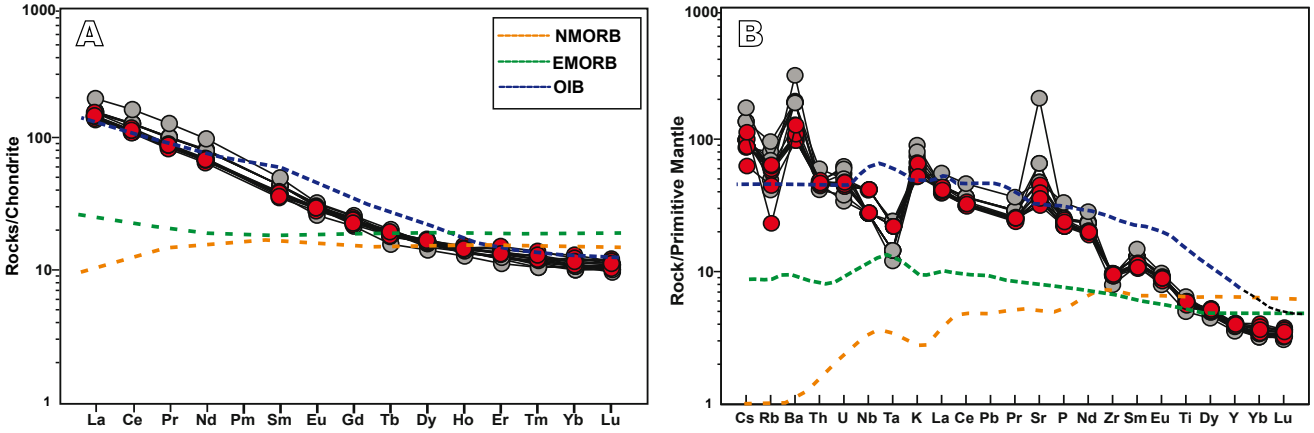

FIGURE 5. A) Chondrite and B) primitive mantle normalized spider diagrams of the Shahr-e-Babak High-Nb basalts (normalization values are from Sun and McDonough, 1989). Symbols are the same as in Figure 4.

(E-MORB) and Normal Mid Oceanic Ridge Basalt (N-MORB).

DISCUSSION

Role of fractional crystallization

The Mg# values of the Shahr-e-Babak HNBs (57,1–66,8) do not show a significant difference from those of the original basaltic magma (65–70) (Frey *et al.*, 1978), suggesting that the basaltic magma did not experienced significant fractional crystallization.

The low SiO_2 content (45.4–49.5wt%), high MgO content (≥6.6wt%), and total FeO content (>11wt%) are also distinctive features that indicate slight fractionation nature of these samples. Thus, the Shahr-e-Babak HNBs probably are not representative of primary melts (Wilson, 1989), but their compositions do not reveal significant modification through fractionation of mantle-derived melts. Considering of the relatively high Ni (155–244ppm) content in the studied HNBs than unfractionated mafic magmas (Ni= 200–450ppm) (Table 1) also rule out the highly fractionated olivine as the important mafic phases in basaltic rocks. Moreover, the studied HNBs show a high content of Cr (234–374ppm) compared to the reported values for the primary magmas (142ppm; Hughes, 1982), which provide a good geochemical indicator of slight clinopyroxene fractionation during magma evolution. These evidence show that they can considered as enough primary to investigate the magma source and genesis in this region.

The elevated concentrations of Ba and Sr together in the samples compared to the average OIB (Fig. 5B) is probably attributed to incompatible behavior of these elements during fractionation of mafic phases (*i.e.* olivine and clinopyroxene). The absence of a Eu anomaly also suggests that they probably crystallized much less than about 18% plagioclase prior to extrusion (John *et al.*, 1968). Geochemical modeling of the studied HNBs (Fig. 6A) suggests a clear olivine and magnetite fractionation during magma evolution. However, these modifications are minor and insignificant.

The La versus La/Yb diagram (Fig. 6B) show that most of the samples follow a positive correlation with the partial melting trend, while three samples are plotted along both partial melting and fractional crystallisation trends and two samples (from KH1) are plotted along fractional crystalization. The studied samples also are plotted as a cluster possibly affected by partial melting, in the high La/Sm ratio versus La concentration (Fig. 6C), imply that these trace elements are more likely controlled by partial melting than fractional crystallization during evolution of magma in this area.

Effects of crustal contamination

It is well known that when hot basaltic magma traverse through continental crust some chemical components from the crust may play a significant role in the petrogenesis of the magma-derived rocks (Ashwal, 2021). The studied HNBs exhibit enrichment in LILE and LREE but depletion in Nb, Ta and HREE, as characteristic feature of magmas in active continental margin volcanism (Nagudi *et al.*, 2003) and subduction zones (Wilson, 2007). Thus, these HNBs may derived from a metasomatized mantle wedge above the subducting oceanic crust with negative anomalies of HFSEs (i.e. Nb and Ti Wilson, 2007) and/or affected via the contamination and magma mixing with crustal material during magma ascent and emplacement (Wilson, 2007).

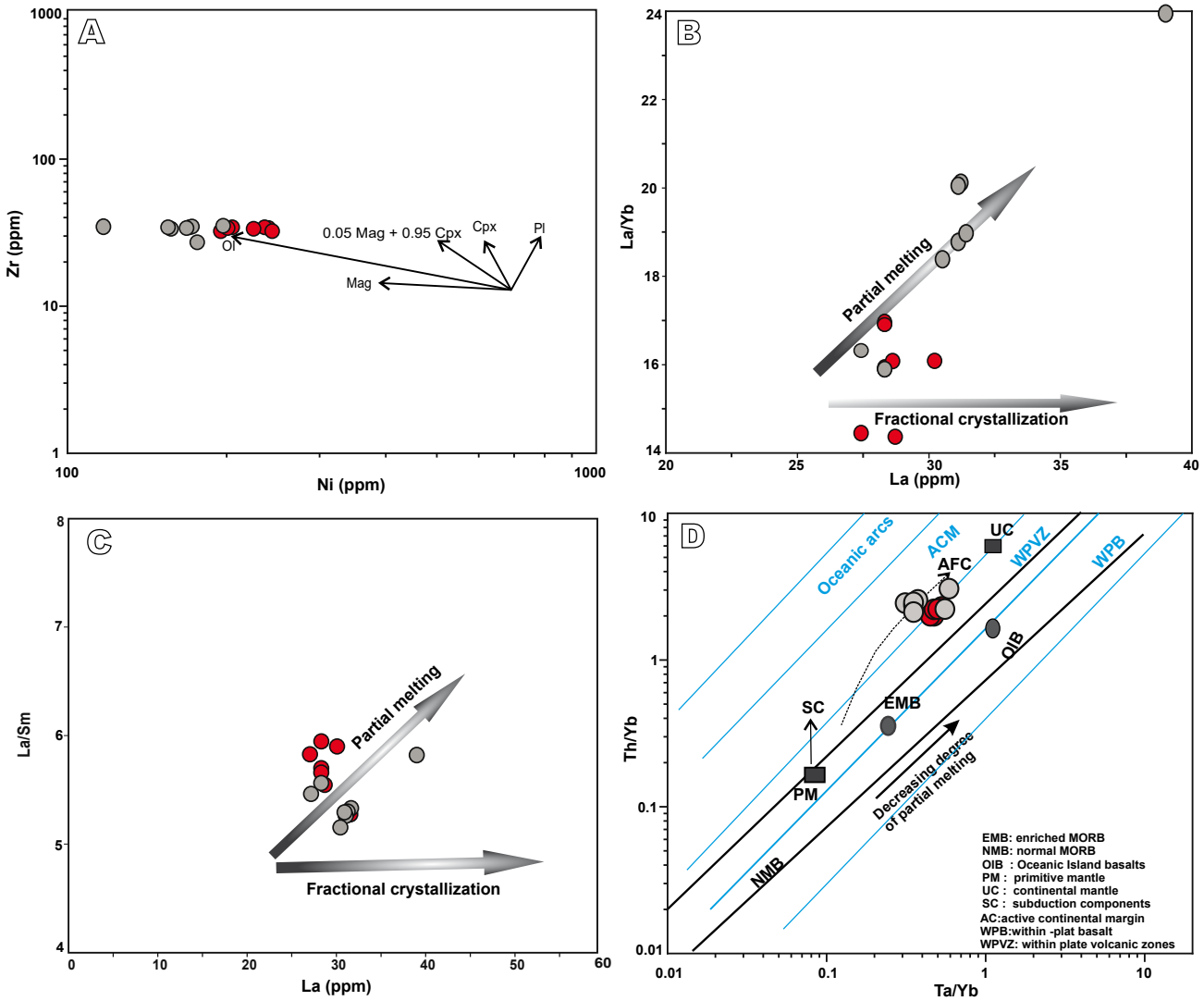

FIGURE 6. A) Fractional crystallization vectors for the studied samples from the Shahr-e-Babak HNBs with crystallization rate in Ni versus Zr diagram. Ol= Olivine, Mag= Magnetite, Pl= Plagioclase, Cpx= Clinopyroxene; B) La versus La/Yb diagram; C) La/Sm versus La diagram for; D) Ta/Yb versus Th/Yb diagram (Pearce, 2008). AFC, Assimilation combined with Fractional Crystallization curve. , EMB (Enriched morb), NMB(Normal morb), OIB(Oceanic island basalt), PM (Primitive mantle)are from Sun and McDonough (1989); UC (Upper crust)is from Taylor and McLennan (1985); Fields for Karacadag and Hatay are from Parlak *et al.* (2000), Field for the basaltic volcanism of the Arabian plate is from Lustrino and Wilson (2007). Western Anatolia field is from Aldanmaz *et al.* (2007). Symbols are the same as in Figure 4.

Trace element ratios have been routinely used to investigate crustal contamination in basaltic rocks. Th/Yb and Ta/Yb ratios are almost independent of fractional crystallization and/or partial melting, thus they can reveal source variations and crustal contamination. Source region metasomatism caused by subduction processes, results enrichment in Th and higher Th/Yb ratios than Ta and Ta/Yb respectively. Crustal contamination also increases Th/Yb ratios relative to Ta/Yb ratios due to the higher abundance of Th relative to Ta in the crustal rocks (Fadaeian *et al.*, 2022). In the Th/Yb versus Ta/Yb diagram (Pearce, 1983) (Fig. 6D), the HNBs are plotted with Th/Yb ratios higher than the mantle array. However, it is difficult to distinguish the effects of crustal contamination on the magma composition from metasomatism caused by subduction components. Thus, the high Th/Yb ratio in most samples is unlikely to be the result of crustal contamination solely.

On the other hand, Th/Ta ratio ranges from 4 to 7, which fall between the original mantle ratio (Th/Ta= 2.3) and continental crustal (Th/Ta= 10) ratio (Sun and McDonough, 1989), which indicates insignificant crustal contamination in the evolution of the HNBs.

Moreover, low Nb/La ratios (<1.0) in the basaltic rocks are a key index and reflect crustal contamination in the magma evolution (Kieffer *et al.*, 2004). The studied HNBs from KH1 location have Nb/La ratios from 1 to 1.1

indicating that crustal signature is insignificant in these rocks, but those basalts from KH2 location with Nb/La ratios from 0.6 to 0.9 reflect some crustal contamination.

In the Nb/Th versus Nb/La (Fig. 7A), and Rb/La versus Th diagrams (Fig. 7B), all the samples plotted close to the mantle composition, ruling out significant crustal contamination. Zr/Nb ratio can be used to determine the influence of continental crust on the mantle derived magma. The Zr/Nb ratio ranges from 3.5 to 5.6, in the HNBs being this range similar to the range observed in the OIB mantle sources (3.2-5), lower than those of continental crust (16.2) and primitive mantle (14.8), and far lower than normal-MORB (30) (Saunders *et al.*, 1988; Weaver, 1991a), which ruled out significant crustal contamination. Therefore, more likely the composition of the studied HNBs was mainly controlled by compositional differences in the source region and by mantle partial melting.

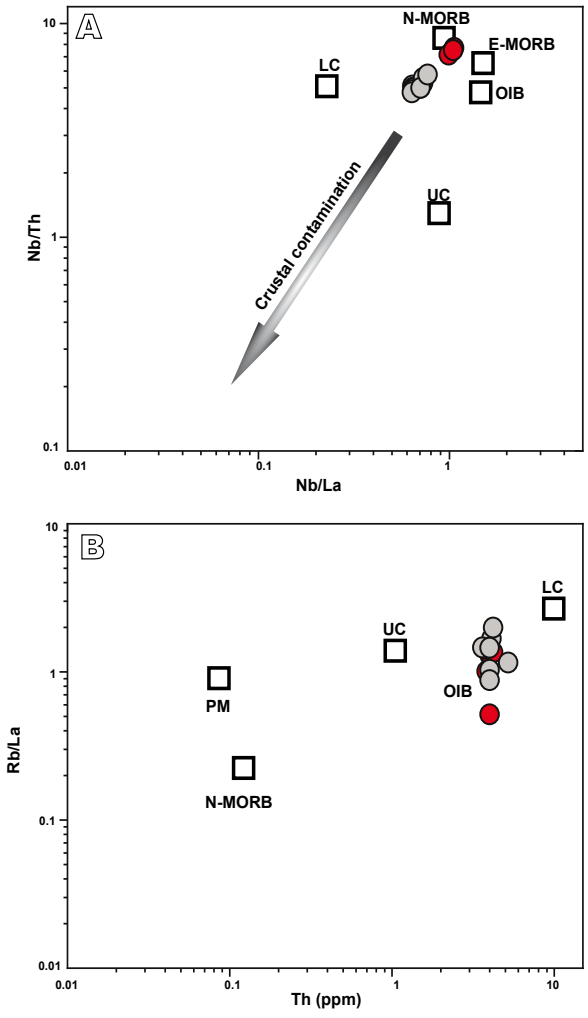

FIGURE 7. A) Nb/La versus Nb/Th diagram (Zhang *et al.*, 2011); B) Th versus Rb/La diagram (Taylor and McLennan, 1981). LC= Lower crust, UC= Upper crust, PM= Primitive mantle Symbols are the same as in Figure 4.

Role of the slab components

The Shahr-e-Babak HNBs formed in a continental margin environment and are different from continental intra-plate basalts in term of trace elements (Fig. 6D). Subduction-related magmas are characterized by high Ba/Nb (>28) and Ba/Ta (>450) ratios (Fitton and Dunlop, 1985; Gill, 1981). These ratios range from 23 to 109 and 720 to 3633, respectively in the studied samples which, indicate that the subduction components play an important role in the source region.

In order to determine the influence of subduction materials on the source of the basaltic samples, we used the Th/Nb versus Ba/Th diagram (Orozco Esquivel *et al.*, 2007) (Fig. 8A). The variable Th/Nb along with variable Ba/Th ratios is resulted from the addition of both hydrous fluid and melt to the source. Similar behaviors are also inferred from Th/Nb versus La/Nb plot (Fig. 8B). The Th/Nb versus La/Nb diagram is used to distinguish between melt (high Th/Nb and low La/Nb) and fluid (low Th/Nb and high La/Nb) components as slab-derived material in the subduction zones. In this diagram, the studied HNBs indicate a transitional nature between the melt and fluid trends (Fig. 8B).

Hastie *et al.* (2013) also developed the Th/La versus (Ce/Ce*)N diagram (Fig. 8C) to determine the slab-derived components in the petrogenesis of arc related magmatic rocks. The studied samples are plotted in the volcanic detritus field on a subvertical trend corresponding to a mixture between continental detritus/GLOSS II and N-MORB. This confirms that the mantle source region has been enriched by melts derived from subducted sediments in the studied area.

According to Ayers (1998), the presence of long-lasting phases containing Nb, Ta, Ti elements such as rutile, sphene, apatite and ilmenite in eclogite-facies rocks in subducted oceanic crust or non-melted mantle wedges can be considered a reason for negative anomalies of compatible elements in the mantle wedge derived magmatism. Therefore, these evidences suggest slab melting also played a critical role in the genesis of the Shahr-e-Babak HNBs.

Source of the Shahr-e-Babak High-Nb basalts

Trace element compositions of Shahr-e-Babak HNBs, especially their enrichment in the LILEs and strong fractionation between LREE and HREE are similar to OIB (Fig. 5B), but they show no obvious negative Nb anomalies or even positive Nb anomalies similar to OIB.

Two different types of HNBs have been proposed in the volcanic arcs: i) HNBs originated from the OIB source

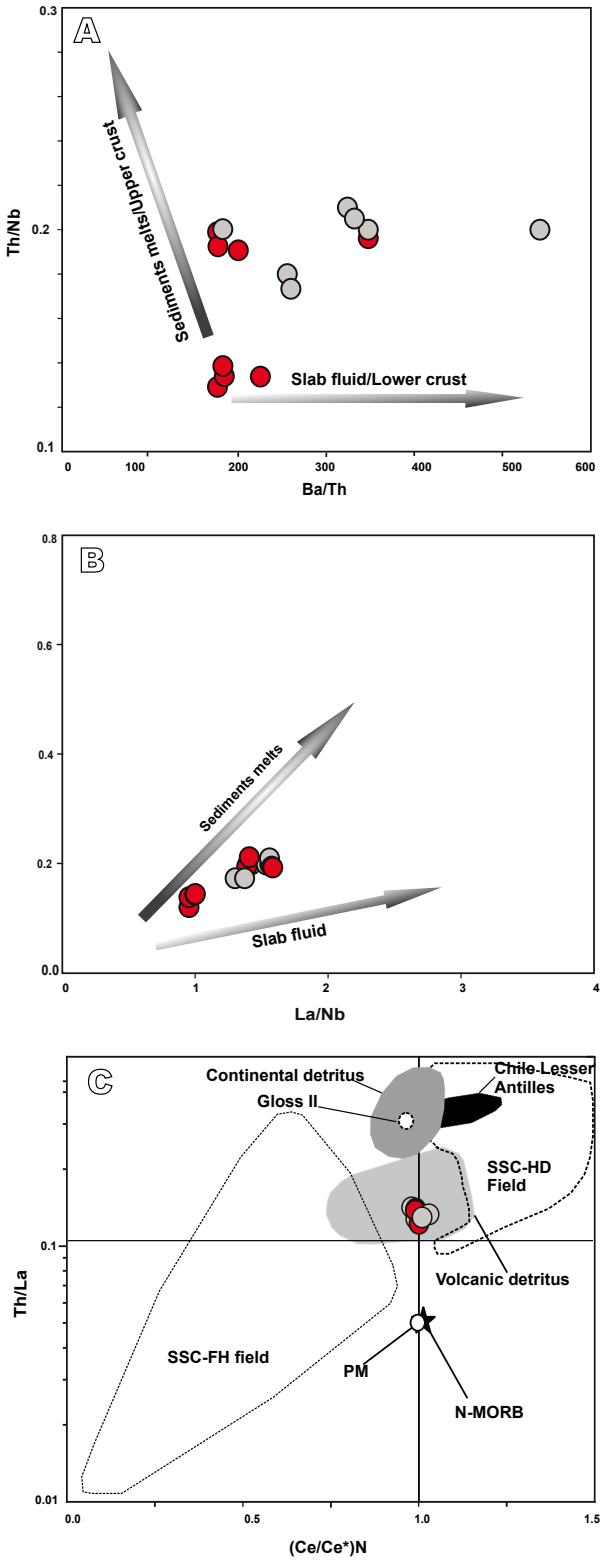

FIGURE 8. A) Ba/Th versus Th/Nb diagram (Anders and Grevesse, 1989) and B) La/Nb versus Th/Nb diagram for discrimination between sediment melts and slab-fluid components in volcanic arcs; C) Ce/Ce* versus Th/La after Hastie *et al.* (2013). Shaded fields are from Hastie *et al.* (2013). SSC-HD, Slow Sediment Clay–Hydrogenous; SSC-FH, Slow Sediment Clay–Fish debris/Hydrothermal. Symbols are the same as in Figure 4.

mantle (similair enriched, OIB-like isotopic and OIB-like trace element signature; Castillo, 2008; Gazel *et al.*, 2011) and ii) HNBs from enriched mantle wedge that was metasomatized by slab-derived adakites in amphibolite or eclogite facies (similair N-MORB like isotopes and OIB-like trace elements; Defant *et al.*, 1992; Imaoka *et al.*, 2014; Straub *et al.*, 2013). The enriched (plume-type) mantle source (first HNB type) is achieved either through influx of asthenospheric mantle through slab windows (Castilli *et al.*, 2008) or mixing between enriched (plume-type) and depleted components within mantle wedge (*e.g.* Macpherson *et al.*, 2010).

HNBs are usually found simultaneously or as younger magmatism with adakites in orogenic belt at least in Iran geology (*e.g.* Azizi *et al.*, 2014; Hastie *et al.*, 2011; Mazhari, 2016). Furthermore, the close association of the high-Nb basaltic rocks with adakites arises the idea that HNBs are usually generated in subduction zones from a depleted mantle wedge (essentially MORB like) metasomatized by adakitic magmatism (Defant and Kepezhinskas, 2001; Hastie *et al.*, 2011; Kepezhinskas *et al.*, 1995; Kepezhinskas *et al.*, 2019; Sajona *et al.*, 1993; Wang *et al.*, 2007).

Adakitic plutonism and volcanism in the vicinity of the studied HNBs have been reported in the Shahr-e-Babak area. The source of adakite series in the Dehaj area are considered as a partial melting product of eclogitized mafic lower crust (Kheirkhah *et al.*, 2013). Adakitic plutonic rocks in northwest of Shahr-e-Babak (Ghadami and Nazarnia, 2022) and the Meiduk and Parkam (Alirezaei *et al.*, 2017) are attributed to partial melting of garnet bearing to amphibolitic lower continental crust and lithospheric mantle respectively. Ghadami *et al.* (2008) suggested a slab melting mechanism for post-collisional Plio-Pleistocene adakitic volcanism from Javazm, northwest of Shahre-Babak. The Plio-Pleistocenic subvolcanic porphyritic andesitic-dacitic domes in Anar- Dehaj (Shaker ardakani, 2016) with adakite signitures also attributed to slab melting and underplating of basaltic magmas under thick Plio-Pleistocene continental crust.

Partial melting of subducting oceanic slab in the amphibolite–eclogite transition (i.e. in low-water fluid conditions) led to titanite stability in the residual slab (König *et al.*, 2010). The residual titanites liberate Nb into a slab melt than Ta preferentially (Zhang *et al.*, 2015). Moreover, rutile also preferentially retains Ta over Nb, beacuse DNb is lower than DTa in rutile/melt pair during high pressure melting (Xiong *et al.*, 2011). Thus Nb will be released into slab derived melt and subsequently, Nb will be enriched in mantle wedge after metasomatism by flux from hot oceanic lithosphere (Zhang *et al.*, 2015). Moreover, adakitic magmas (slab melt) are characterized by high Sr/Y

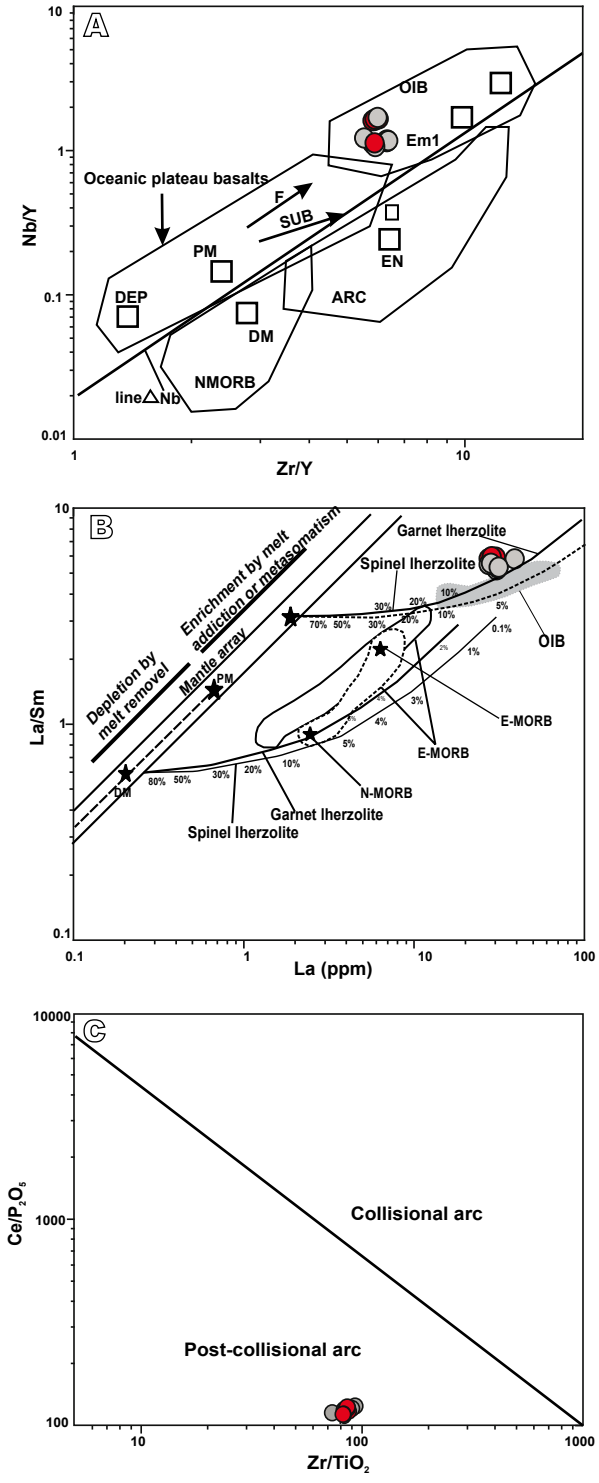

FIGURE 9. A) Zr/Y versus Nb/Y diagram; UC= Upper Continental crust; PM= Primitive mantle; DM= Depleted mantle; HIMU= High Mu (U/Pb) source; EM1 and EM2= Enriched mantle sources; ARC= Arc related basalts; NMORB= Normal ocean ridge basalt; OIB= Oceanic island basalt; DEP= Deep depleted mantle; EN= Enriched component; F Arrow= effects of batch melting and SUB= Subduction effects from Weaver (1991) and Condie (2003). B) La versus La/Sm diagram (Aldanmaz *et al.*, 2000). OIB and MORB values are from Sun and McDonough (1989); C) Zr/TiO_2 versus Ce/P_2O_5 tectonic setting discrimination diagrams (Muller *et al.*, 1997). Symbols are the same as in Figure 4..

and (La/Yb)N ratios and low YbN values. Thus, when the mantle wedge is metasomatized by adakitic magmatism, it also should show similar chemical compositions to adakite (Tang *et al.*, 2010; Wang *et al.*, 2007). Chemically, the studied HNBs also show similarity to a mantle wedge metasomatized by adakitic melts with high Sr/Y.

As discussed in the crustal contamination section, trace elements have not been affected by significant fractional crystallization. Therefore, we used trace and rare earth element ratios as key parameters to determine the studied HNBs source. These samples with low Zr/Nb coupled with high Zr/Y and Nb/Y ratios (3.5–5.6, 5.5–6.3 and 1.1–1.7 respectively), are different with those of Depleted Mantle (DM) and its related melts (*e.g.* N-MORB and oceanic arc basalt) but resemble the source of OIB.

Different sources have been proposed for OIB magmas. For example many researchers consider the fertile lower mantle peridotite (*e.g.* Woodhead, 1996), while others suggest a lithospheric mantle source contaminated by carbonatite/plume derived melts as source the OIB magmas (Mazahari, 2015; Nakamura and Tatsumoto, 1988). Plotting of the samples in the Zr/Y versus Nb/Y diagram (Fig. 9A) suggests that they are more likely derived from OIB-like mantle. However, other distinct geochemical index of the studied HNBs, i.e. Nb/U (14.9-32.3 with average 23.7), displays compositional differences with both N-MORB and OIB (Nb/U 50; Hofmann, 2004).

In the La/Sm versus La modeling diagram (Aldanmaz *et al.*, 2000) (Fig. 9B), the Shahr-e-Babak HNBs with high MgO (>6.6) plotted in the garnet lherzolite consistent with the 5–7% partial melting. In the studied samples, the trace elements and REE ratios contain Dy/YbCN> 1 (= 1.3 to 1.5), low to moderate Y (<25ppm), low Yb< (2ppm), Y/Yb= 9.3-10.8 and (Ho/Yb)N= 1.1-1.3, suggesting that garnet (=Y/Yb> 10 and (Ho/Yb)N> 1.2) rather than spinel was a residual phase in the mantle source during the partial melting processes in the studied area (Ge *et al.*, 2002).

The similarity between this study and recent works (*e.g.* Castillo *et al.*, 2007; Sajona *et al.*, 1996) demonstrate that unlike OIB lavas, HNBs are not generated from a pure mantle plume source or metasomatism of the mantle by carbonatite/ mantle plume melts. Consequently, Shahr-e-Babak HNBs were generated within garnet lherzolite mantle wedge (in asthenospheric mantle) metasomatized by fluids, overlying sediments and adakitic melt derived from subducted Neotethys oceanic crust.

Ce/Yb ratio in basaltic rocks is very sensitive to the lithospheric thickness (Ellam, 1992) due to their high stability during fractional crystalization. High Ce/Yb ratios

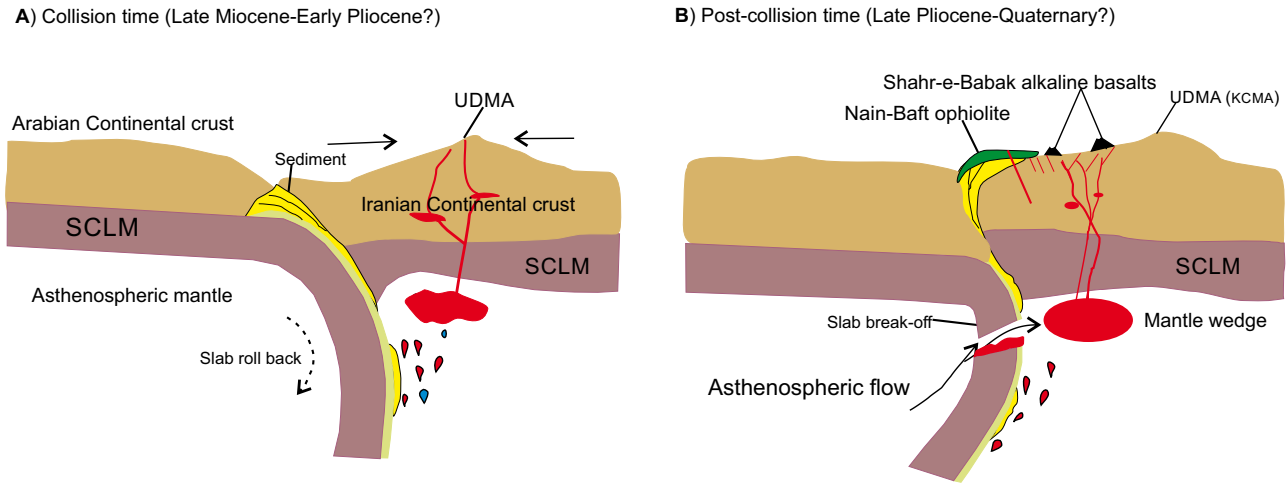

FIGURE 10. Geodynamic model of change of tectonic regime from A) collisional time to B) post-collisional time. SCLM= Subcontinental Lithospheric Mantle.

(29.2-49.3) in the studied samples also correspond to smaller melt fractions and/or garnet control (depth higher than 110–120km in the studied area).

In summary, based on the combined interpretation of gravity, topography data sets (Monilaro *et al.*, 2005), geophysical-petrological methodology (Tunnini *et al.*, 2015), and trace elements geochemistry (Ce/Yb, and Nb/La (0.6 to1.1)), it appears that the mantle source for the HNBs in Shahr-e-Babak area is located in the upper portion of the mantle asthenosphere.

GEODYNAMIC IMPLICATIONS

Post-collision alkaline magmatism was produced by a complex combination of geodynamic and petrogenetic processes during the evolution of the Alpine–Himalayan collision belt, from west-to-east though Turkey, Iran and into Pakistan (Allen *et al.*, 2013; Azizi *et al.*, 2014; Mazahari, 2015; Neill *et al.*, 2015).

There is not consensus on the timing of the onset collision of the Arabia and Eurasia; it has been suggested the Late Cretaceous (Alavi, 1994; Berberian and King, 1981), the middle Miocene–Pliocene (Berberian and Berberian, 1981; Stöcklin, 1968), and the late Miocene–Pliocene (McQuarrie *et al.*, 2003). Post-collisional alkaline rocks in the UDMA are reported locally as alkaline and shoshonitic OIB like volcanic rocks in Saray (Shafaii Moghadam *et al.*, 2014), Qom-Aran (Amidi, 1977; Emami, 1981), Moghan (Amraee *et al.*, 2019), Saveh (Caillet *et al.*, 1978), Marand (Ahmadzadeh *et al.*, 2010), Ahar (Dabiri *et al.*, 2011), Qom-Baft, and Anar (Ahmadian *et al.*, 2014; Saadat *et al.*, 2010).

Post-collisional magmatic activites (volcanism and plutonism) in NW of the KCMA are reported as adakite-like rocks (Alirezaei *et al.*, 2017; Ghadami *et al.*, 2008; Ghadami *et al.*, 2009; Ghadami, 2016; Kheirkhah *et al.*, 2020), alkaline volcanism (Amidi, 1984; Hassanzadeh, 1993; Hosseini *et al.*, 2009; Moradian, 1997), Late Pliocene to Quaternary shoshonitic rocks in Bardsir (Atapour, 1994), the Quaternary Qal'eh Hasan Ali Maars (Milton, 1977), adakite-like porphyritic granodiorites of the Kuh-e Panj-type (Haschke *et al.*, 2010; Hou *et al.*, 2011; Shafiei *et al.*, 2009), 1 to 2Ma Anar volcanic rocks (Pang *et al.*, 2016) and Pleistocene alkali basalts in the south west of Anar area (Hosseini *et al.*, 2009). The geochemical characteristics of the studied Shahr-e-Babak HNBs also represent post-collision magamtism in a continental arc setting in the KCMA (Figs. 6D; 9C).

The most efficient geodynamic mechanisms during generation of post-collisional alkaline and HNBs in subduction zones are mantle plumes and/or upwelling asthenospheric mantle (*e.g.* Liu *et al.*, 2018; Niu *et al.*, 2012; Wang *et al.*, 2015) associated with local extension regime or lithospheric delamination mechanisms (Guo *et al.*, 2007), and/or the opening of slab detachment (slab break-off) within modern arc-trench systems (Gazel *et al.*, 2009; Gill, 1984; Keskin, 2003) Both proposed mechanisms provide a way to initiate partial melting of mantle wedge.

A mantle plume usually leads to a dynamic uplift over an area 1000–2000km in diameter (Hill *et al.*, 1992; Ritter and Christensen, 2007), which is not seen in the studied area. Lithospheric delamination leads to the upwelling of the hot asthenosphere and melting of the asthenosphere in shallow depth close to the Moho, but the Shahr-e-Babak HNBs formed at considerable depth (>110km)

and also the geophysical studies (Clark, 1993; Saric and Mijalkovic 1973) also show that the crust beneath the NW of the KCMA has a thickness of 45–55km. Hence, the lithospheric delamination mechanism is not also favoured for the genesis of the studied HNBs.

The occurrence of adakitic volcanism in the vicinity of the Plio-Quaternary HNBs in Shahr-e-Babak area shows that break-off episodes played an important role in their generation following a Paleogene slab rollback as suggested for the UDMA mamatism (Ghorbani *et al.*, 2014; Moradi *et al.*, 2021; Verdel *et al.*, 2011). On the basis of the data presented herein and the occurrence of adakitic rocks in the NW of the KCMA, the following scenario could be suggested for HNBs in this area: After collision of the Arabian and Iranian blocks caused by slab pull force during subduction of the Neotethyan oceanic lithosphere, the slab break-off occurred due to an approximately 30% decrease in the velocity of the Arabian plate (Mouthereau *et al.*, 2012; Verdel *et al.*, 2011). A modeling from Molinaro *et al.* (2005) based on the gravity, geoid and topography data sets also highlights a thinned lithospheric mantle below the KCMA which is attributed to recent slab break-off. Oceanic slab break-off provides a reasonable explanation for the origin of post-collisional magmatism (Davies and von Blanckenburg, 1995).

Slab break-off had led to thermal perturbation by upwelling of hot asthenosphere which has prepared the appropriate conditions for partial melting of amphibolite or eclogite from detached subducting slab (Berberian, 1981; Martin, 2005) to produce adakitic magmas (Ahmadzadeh *et al.*, 2010; Azizi *et al.*, 2014; Ghadami *et al.*, 2008; Ghasemi and Talbot, 2006; Kouhestani *et al.*, 2017; Omrani *et al.*, 2008). Subsequently the adakitic liquids metasomatized mantle wedge for a long period of time. The thermal flux originating from the deep asthenosphere and uprising through the oceanic slab break-off, probably provided the excess heat, triggered the partial melting of metasomatized mantle wedge, and produced the HNB magmas in the Shahr-e-Babak during Plio-Quaternary (Fig. 10). This geodynamic model has been proposed already for other post-collisional alkaline magmatic rocks widely distributed throughout the Tethyan orogenic belt (*e.g.* Aguillon-Robles *et al.*, 2001; Azizi *et al.*, 2014; Kepezhinskas *et al.*, 2022; Hastie at al., 2011; Hussain *et al.*, 2020; Mazhari, 2015; Wang *et al.*, 2008; Zhu *et al.*, 2018).

It is noteworthy that extensional regime usually suggeted during post-collision magmatism in Zagros orogeny due to asthenospheric mantle upwelling oceanic plate fallowing rollback and subsequent slab break-off (Azizi *et al.*, 2014; Boccaletti *et al.*, 1976; Razavi and Sayyareh; 2010).

The time span between initiation of continental collision and slab break-off varies from 10 to 20 million years for young (weak) and old (strong) slabs, respectively (Van Hunen and Allen, 2011). Transition from tholeiitic-calc-alkaline (Noorizadeh *et al.*, 2018) to alkaline (Taghipour, 2007), adakitic magmatism (Ghadami *et al.*, 2008; Shaker Ardakani, 2016), and finally the occurrence of OIB-like asthenospheric mantle indicates the maturation of arc magmatism (Zarasvandi *et al.*, 2015).

CONCLUSIONS

i) The post-collision Plio-Quaternary Shahr-e-Babak HNBs contain mainly olivine, clinopyroxene and plagioclase, and generated in a continental margin (extensional) setting. These alkaline basalts, show a high Nb content (>20) and geochemical features comparable with those of OIB.

ii) The geochemical signatures of the samples suggest that the HNBs derived from a low degree partial melting (<5-7%) of the garnet peridotite mantle wedge metasomatized by adakitic melts at considerable depth (>110).

iii) A slab break-off model is suggested to explain direct asthenosphere heat flow for melting of subducting slab to produce adakitic slab melts and also trigger mantle source of the HNBs.

ACKNOWLEDGMENTS

We are thankful to the geology department of Shahid Bahonar University for their help during field working. We appreciate editor and anonymous reviewers for their constructive comments and suggestions, which helped to improve the manuscript.

REFERENCES

Agard, P., Omrani, J., Jolivet, L., Whitechurch, H., Vrielynck, B., Spakman, W., Monié, P., Meyer, B., Wortel, R., 2011. Zagros orogeny: a subduction-dominated process. Geological Magazine, 148, 692-725.

Aguillon-Robles, A., Calmus, T., Benoit, M., Bellon, H., Maury, R.C., Cotton, J., Bourgois, J., Michard, F, 2001. Late Miocene adakites and Nb-enriched basalts from Vizcaino Peninsula, Mexico: Indicators of East Pacific Rise subduction below southern Baja California? Geology, 29, 531-534.

Ahmadian, J., Murata, M., Nadimi, A., Ozawa, H., Takeshi, K., 2014. Recent tectonic activity of Iran deduced from young magmatism evidences. Bulletin of Center for Collaboration in Community Naruto University of Education, 28, 23-38.

Ahmadzadeh, G., Jahangiri, A., Lentz, D., Mojtahedi, M., 2010. Petrogenesis of Plio-Quaternary post-collisional ultrapotassic

volcanism in NW of Marand, NW Iran. Journal of Asian Earth Science, 39, 37-50.

Alavi, M., 1994. Tectonics of the Zagros orogenic belt of Iran: new data and interpretations. Tectonophysics, 229, 211-238.

Aldanmaz, E., Pearce, J.A., Thirlwall, M.F., Mitchell, J.G., 2000. Petrogenetic evolution of late Cenozoic, post-collision volcanism in western Anatolia, Turkey. Volcanology and Geothermal Research, 102, 67-95.

Alirezaei, A., Arvin, M., Dargahi, S., 2017. Adakite-like signature of porphyry granitoid stocks in the Meiduk and Parkam porphyry copper deposits, NE of Shahr-e-Babak, Kerman, Iran: Constraints on geochemistry. Ore Geology Reviews, 88, 370-383.

Allen, M., Jackson, J., Walker, R., 2004. Late Cenozoic reorganization of the Arabia–Eurasia collision and the comparison of short-term and long-term deformation rates. Tectonics, 23, TC 2008.

Allen, M.B., Kheirkhah, M., Neill, I., Emami, M.H., McLeod, C.L., 2013. Generation of arc and within-plate chemical signatures in collision zone magmatism: quaternary lavas from Kurdistan Province, Iran. Petrology, 54, 887-911.

Amidi, S.M., 1977. Étude géologique de la région de Natanz-Surk (Iran, Central). Ph.D. thesis. France, Université Grénoble, 316pp.

Amidi, S.M., Emami, M.H., Michel, R., 1984. Alkaline character of Eocene volcanism in the middle part of central Iran and its geodynamic situation. Geologische Rundschau, 73, 917-932.

Amraee, A., Zareisahamieh, R., Moayyed, M., Ahmadikhalaji, A., AzimZadeh, A.M., Santos, J.F., 2019. Peshtasar basalts: An example of post-collision basalts in sedimentary basin of Moghan, NW Iran. Journal of Earth System Science, 128(3), 1-22.

Atapour, H., 1994. Petrology and geochemistry of shoshonitic association of Goud-e-Biabani Bardsir area, Kerman province (In Persian). M.Sc. Thesis. Shahid Bahonar University of Kerman, 244pp.

Azizi, H., Jahangiri, A., 2008. Cretaceous subduction-related volcanism in the northern Sanandaj-Sirjan Zone, Iran. Geodynamics, 45, 178-190.

Azizi, H., Asahara, Y., Tsuboi, M., 2014. Quaternary high-Nb basalts: Existence of young oceanic crust under the Sanandaj–Sirjan zone, NW Iran. International Geology Review, 56(2), 167-186.

Bamorovat, M., Dargahi, S., Arvin, M., 2014. Mineralogy, petrology and tectonic setting of Neogene basaltic magmatism in Dehaj- Javazm area, northwest of Shahre-Babak. 21th Iranian conference on crystallography and mineralogy.

Berberian, F., Berberian, M., 1981. Tectono-plutonic episodes in Iran. In: Gupta, H.K., Delany, F.M. (eds.). Zagros-Hindu Kush–Himalaya Geodynamic Evolution. Washington DC, American Geophysical Union, 3, 5-32.

Berberian, M., King, G.C.P., 1981. Towards a paleogeography and tectonic evolution of Iran. Canadian Journal of Earth Sciences, 18, 210-265.

Caillet, C., Dehlavi, P., Martel-Jantin, B., 1978. Géologie de la région de Saveh (Iran). Contribution a l'étude du volcanisme et du plutonism Tertiaires de la zone de l'Iran Central (in french). Thèse de Doctorat de Specialities. Grenoble (France), Université Grenoble, 325pp.

Carlson, R.W., Pearson, D.G., James, D.E., 2005. Physical, chemical, and chronological characteristics of continental mantle. Reviews of Geophysics, 43, 1-24.

Castillo, P.R., Solidum, R.U., Punongbayan, R.S., 2002. Origin of high field strength element enrichment in the Sulu Arc, southern Philippines, revisited. Geology, 30, 707-710.

Castillo, P.R., Rigby, S.J., Solidum, R.U., 2007. Origin of high field strength element enrichment in volcanic arcs: Geochemical evidence from the Sulu Arc, southern Philippines. Lithos, 97, 271-288.

Castillo, P.R., 2008. Origin of the adakite–high-Nb basalt association and its implications for post subduction magmatism in Baja California, Mexico. Geological Society of America Bulletin, 120, 451-462.

Castillo, P.R., 2012. Adakite petrogenesis. Lithos, 134, 304-316.

Dabiri, R., Emami, M.H., Mollaei, H., Chen, B., Abedini, M., Rashidnejad, N., Ghaffari, M., 2011. Quaternary post-collision alkaline volcanism NW of Ahar (NW Iran): Geochemical constraints of fractional crystallization process. Geologica Carpathica, 62, 547-562.

Davies, J.H., von Blanckenburg, F., 1995. Slab breakoff: a model of lithosphere detachment and its test in the magmatism and deformation of collisional orogens. Earth Planetry Science Letter, 129, 85-102.

Defant, M.J., Jackson, T.E., Drummond, M.S., De Boer, J.Z., Bellon, H., Feigenson, M.D., Maury, R.C., Stewart, R.H., 1992. The geochemistry of young volcanism throughout western Panama and southeastern Costa Rica: An overview. London, The Geological Society, 149, 569-579.

Defant, M.J., Kepezhinskas, P., 2001. Evidence suggests slab melting in arc magmas: EOS. Transactions of the American Geophysical Union, 83(23), 62-69.

Dercourt, J., Zonenshine, L.P., Ricou, L.E., Kazmin, V.G., Le Picon, X., Knipper, A.L., Grandjacquet, C., Sbortshikov, I.M., Geyssany, J., Lepveier, C., 1986. Geological evolution of the Tethys belt from the Atlantic to the Pamirs since the Lias. Tectonophysics, 123, 241-315.

Dewey, J.F., Pitman, W.C., Ryan, W.B.F., Bonnin, J., 1973. Plate Tectonics and the Evolution of the Alpine System. Geological Society of America Bulletin, 84, 3137-3180.

Dimitrijevic, M.D., 1973. Geology of Kerman Region. Geology Survey of Iran, Report No. 52, 334pp.

Ellam, R., 1992. Lithospheric thickness as a control on basalt geochemistry. Geology, 20(2), 153-156.

Emami, M.H., 1981. Géologie de la région de Qom-Aran (Iran): Contribution a l'étude dynamique et géochimique du volcanisme Tertiaire de l'Iran Central. Ph.D. Thèse. France, Université Grenoble, 489pp.

Fadaeian, M., Jahangiri, A., Ao, S., Kamali, A.A., Xiao, W., 2022. Geochemistry and Petrogenesis of Shoshonitic Dyke Swarm

in the Northeast of Meshkinshahr, NW Iran. Minerals, 12(309), 2-27.

Fitton, J.G., Dunlop, H.M., 1985. The Cameroon Line, West Africa, and its bearing on the origin of oceanic and continental alkali basalts. Earth and Planetary Science Letters, 72, 23-38.

Frey, F.A., Green, D.H., Roy, S.D., 1978. Integrated models of basalt petrogenesis: A study of quartz tholeiites to olivine melilitites from South Eastern Australia utilizing geochemical and experimental petrological data. Petrology, 19, 463-513.

Ghadami, G.R., Moradian, A., Mortazavi, M., 2008. Post-Collisional Plio-Pleistocene Adakitic volcanism in Centeral Iranian Volcanic Belt: Geochemical and geodynamic implications. Islamic Republic of Iran, Journal of Sciences, 19, 223-236.

Ghadami, G.R., 2009. Petrography, geochemistry and petrogenesis of intrusive and subvolcanic masses (adakitic) in Northwest Share-Babak, Kerman. Unpublished Ph.D. Thesis. Islamic Republic of Iran, Shaheed Bahonar University of Kerman, 334pp.

Ghadami, G.R., 2016. Geochemical and Petrogenesis of Granitoides rocks in South-East of Centeral Iranian Volcanic Belt, North-West of Share-Babak, Kerman Province, Iran. Journal of Tethys, 4(4), 295-311.

Ghadami, G.R., Nazarinia, A., 2022. Adakite signatures in granitoids northwest of Shahr-e-Babak, Kerman, Iran: constraints from geochemistry. Journal of mineralogy and geochemistry, 197(3), 263-283.

Gazel, E., Carr, M.J., Hoernle, K., Feigenson, M.D., Szymanksi, D., Hauff, F., Bogaard, P., 2009. The Galapagos-OIB signature in southern Central America: mantle refertilization by arc–hot spot interaction. Geochemistry, Geophysics, Geosystem, 10(2), 1-32.

Ge, X.Y., Li, X.H., Chen, Z.G., Li, W.P., 2002. Geochemistry and petrogenesis of Jurassic high Sr/low Y granitoids in eastern China: constrains on crustal thickness. Chinese Science Bulletin, 47, 962-968.

Ghasemi, A., Talbot, C.J., 2006. A new tectonic scenario for the Sanandaj–Sirjan zone (Iran). Journal of Asian Earth Sciences, 26, 683-693.

Ghorbani, M.R, Graham, I.T., Ghaderi, M., 2014. Oligocene-Miocene geodynamic evolution of the central part of Urumieh-Dokhtar Arc of Iran. International Geology Review, 56, 1039-1050.

Glennie, K.W., 2000. Cretaceous tectonic evolution of Arabia's eastern plate margin: A tale of two oceans. In: Abdulrahman, S., Alsharhan, Scott, R.W. (eds.), Middle East models of Jurassic/Cretaceous carbonate systems. Society of Economic Paleontologists and Mineralogists, 69 (Special Publication), 9-20.

Gill, J.B., 1981. Orogenic Andesites and Plate Tectonics. Minerals and Rocks, 16, 390pp.

Gill, J.B., 1984. Sr-Nd-Pb isotopic evidence that both MORB and OIB sources contribute to oceanic island arc magmas in Fiji. Earth and Planetary Science Letters, 68, 443-458.

Guo, F., Nakamura, E., Fan, W.M. Kobayoshi, K., Li, C.W., 2007. Generation of Paleocene adakitic andesites by magma mixing, Yanji area, NE China. Journal of Petrology, 48, 661-692.

Haschke, M., Ahmadian, J., Murata, M., McDonald, I., 2010. Copper mineralization prevented by arc-root delamination during Alpine–Himalayan collision in Central Iran. Economic Geology, 105, 855-865.

Hassanzadeh, J., 1993. Metallogenic and Tectonomagmatic Events in the SE Sector of the Cenozoic Active Continental Margin of Iran (Shahre-Babak Area, Kerman Province). Ph.D Thesis. Los Angeles, University of California, unpublished, 204pp.

Hastie, AR., Mitchell, S.F., Kerr, A.C., Minifie, J., Millar, I.L., 2011. Geochemistry of rare high Nb basalt lavas: are they derived from a mantle wedge metasomatized by slab melts? Geochimica et Cosmochimica Acta, 75, 5049-5072.

Hastie, A.R., Mitchell, S.F., Treloar, P.J., Kerr, A.C., Neill, I., Barfod, D.N., 2013. Geochemical components in a Cretaceous island arc: The Th/La–(Ce/Ce*)Nd diagram and implications for subduction initiation in the inter-American region. Lithos, 162-163, 57-69.

Hill, R.I., Campbell, I.H., Davies, G.F., Griffiths, R.W., 1992. Mantle plumes and continental break-up. Earth and Planetary Science Letters, 104, 398-416.

Hosseini, S.Z., Arvin, M., Oberhansli, R., Dargahi, S., 2009. Geochemistry and Tectonic Setting of Pleistocene Basaltic Lava Flows in the Shahre-Babak Area, NW of Kerman, Iran: Implication for the Evolution of Urumieh- Dokhtar Magmatic Assemblage. Islamic Republic of Iran, Journal of Sciences, 20(4), 331-342.

Hosseini, S.Z., 2016. Geochemistry, petrogenesis and tectonic setting of the Sarcheshmeh Eocene mafic lava flows, Southwest of Rafsanjan. Geoscience, 25(100), 209-220.

Hou, Z., Zhang, H., Pan, X., Yang, Z., 2011. Porphyry Cu (Mo–Au) deposits related to melting of thickened mafic lower crust: examples from the eastern Tethyan metallogenic domain. Ore Geology Reviews, 39(1-2), 21-45.

Hughes, C.J., 1982. Igneous Petrology. Amsterdam, Elsevier, 420pp.

Hussain, A., Zhao, K.D., Arif, M., Palmer, M.R., Chen, W., Zhang, Q., Li, Q., Jiang, S.Y., Girei, M.B., 2020. Geochronology, mineral chemistry and genesis of REE mineralization in alkaline rocks from the Kohistan Island Arc, Pakistan. Ore Geology Reviews, 126, 103749.

Imaoka, T., Nakashima, K., Kamei, A., Itaya, T., Ohira, T., Nagashima, M., Kono, N., Kiji, M., 2014. Episodic magmatism at 105 Ma in the Kinki district, SW Japan: Petrogenesis of Nb-rich lamprophyres and adakites, and geodynamic implications. Lithos, 184-187, 105-131.

Jahangiri, A., 2007. Post-Collisional Miocene Adakitic Volcanism in NW Iran: Geochemical and Geodynamic Implications. Journal of Asian Earth Sciences, 30, 433-447.

Kepezhinskas, P.K., Defant, M.J., Drummond, M.S., 1995. Na metasomatism in the sub-arc mantle by slab melt-peridotite interaction: Evidence from mantle xenoliths in the Kamchatka arc. Journal of Petrology, 36, 1505-1527.

Kepezhinskas, P., Kepezhinskas, N., Berdnikov, N., 2019. Gold, palladium and platinum enrichments in arcs: Role of mantle

wedge, arc crust and halogen-rich slab fluids. Tomsk (Russia), Proceedings of the E3S Web Conference, 98, 1-5.

Kepezhinskas, P., Berdnikov, N., Kepezhinskas, N., Konovalova, N., 2022. Adakites, High-Nb Basalts and Copper–Gold Deposits in Magmatic Arcs and Collisional Orogens: An Overview. Geosciences, 12, 29, 2-60.

Keskin, M., 2003. Magma generation by slab steepening and breakoff beneath a subduction-accretion complex: an alternative model for collision-related volcanism in Eastern Anatolia, Turkey. Geophysical Research Letters, 30, 1-4.

Khaksar, T., Rashidnejad-Omran, N., Chen, F., Song, S., Li, S.h.Q., Ghaderi, M., 2020. Zircon U-Pb ages and magmatic history of the Kashan plutons in the central Urumieh-Dokhtar magmatic arc, Iran: Evidence for Neotethyan subduction during the Paleogene-Neogene. Earth Science, 31(1), 53-68.

Kheirkhah, M., Neill, I., Allen, M.B., Ajdari, K., 2013. Small-volume melts of lithospheric mantle during continental collision: Late Cenozoic lavas of Mahabad, NW Iran. Journal of Asian Earth Sciences, 74, 37-49.

Kieffer, B., Arndt, N., Lapierre, H., Bastien, F., Bosch, D., Pecher, A., Yirgu, G., Ayalew, D., Weis, D., Jerram, D.A., Keller, F., Meugniot, C., 2004. Flood and shield basalts from Ethiopia: magmas from the African Superswell. Journal of Petrology, 45, 793-834.

König, S., Schuth, S., 2010. Deep melting of old subducted oceanic crust recorded by superchondritic Nb/Ta in modern island arc lavas. Earth Planetry Science Letters, 301, 265-274.

Kouhestani, H., Ghaderi, M., Emami, M.H., Meffre, S., Kamenetsky, V., McPhie, J., Zaw, K., Nasiri Bezenjani, R., 2017. Compositional characteristics and geodynamic significance of late Miocene volcanic rocks associated with the Chah Zard epithermal gold–silver deposit, southwest Yazd, Iran. Island Arc, 27(1), 1-15.

LeBas, M.J., Lemaitre, R.W., Streckeisen, A., Zanettin, B., 1986. A Chemical Classification of Volcanic-Rocks Based on the Total Alkali Silica Diagram. Journal of Petrology, 27(3), 745-75.

Le Maitre, R.W. (ed.), 2002. Igneous Rocks: A Classification and Glossary of Terms. Recomentations of the International Union of Geological Sciences Subcommission on the Systematics of Igneous Rocks. Cambridge, Cambridge University Press, 236pp.

Liègeois, J.P., 1998. Preface-some words on the post-collisional magmatism. Lithos, 45, 15-17.

Liu, H., Li, Y., Wu, L., Huangfu, P., Zhang, M., 2018. Geochemistry of high-Nb basalt-andesite in the Erguna Massif (NE China) and implications for the early Cretaceous back-arc extension. Geological Journal, 54, 291-307.

Lustrino, M., Wilson, M., 2007. The Circum-Mediterrane an Anorogenic Cenozoic Igneous Province. Earth-Science Review, 81, 1-65.

Mazhari, S.A., 2016. Petrogenesis of adakite and high□Nb basalt association in the SW of Sabzevar zone, NE of Iran: Evidence for slab melt-mantle interaction. African Earth Sciences, 116, 170-181.

McQuarrie, N., Stock, J.M., Verdel, C., Wernicke, B.P., 2003. Cenozoic evolution of Neotethys and implications for the causes of plate motions. Geophysical Research Letter, 30(20), 1-6.

Macpherson, C.G., Chiang, K.K., Hall, R., Nowell, G.M., Castillo, P.R. Thirlwall, M.F., 2010. Plio-Pleistocene intra-plate magmatism from the southern Sulu Arc, Semporna peninsula, Sabah, Borneo: Implications for high-Nb basalt in subduction zones. Volcanology and Geothermal Research, 190, 25-38.

Martin, H., Smithies, R.H., Rapp, R., Moyen, J.F., Champion, D., 2005. An overview of adakite, tonalite-trondhjemite-granodiorite (TTG), and sanukitoid: Relationships and some implications for crustal evolution. Lithos, 79, 1-24.

Milton, D.J., 1977. Qal'eh Hasan Ali maars, central Iran. Bulletin Volcanologique, 40(3), 201-208.

Mohajjel, M., Fergusson, C., 2000. Dextral transpression in Late Cretaceous continental collision Sanandaj-Sirjan Zone, western Iran. Structural Geology, 22, 1125-1139.

Mohajjel, M., Fergusson, C.L., Sahandi, M.R., 2003. Cretaceous–Tertiary convergence and continental collision, Sanandaj–Sirjan Zone, western Iran. Journal of Asian Earth Science, 21, 397-412.

Moinvaziri, H., Ahmadi, A., 1991. Petrography and petrology of igneous rocks (in Persian). Tehran, Tehran University Press, 539pp.

Molinaro, M., Zeyen, H., Laurencin, X., 2005. Lithospheric structure beneath the southeastern Zagros Mountains, Iran: recent slab break-off? Terra Nova, 17, 1-6.

Moradi, S., Ghorbani, M.R., Jiang, S.Y., Christiansen, E., 2021. Mafic to intermediate composition intrusions from the Kahak area, central Urumieh-Dokhtar arc of Iran: transition from Eocene to Miocene intra-arc extensional magmatism. Mineralogy and Petrology, 115, 445-466.

Moradian, A., Peacock, S.M., Rushmer, T., 1997. Geochemistry, geo-chronology and petrography of feldspathoid bearing rocks in Urumieh-Dokhtar Volcanic Belt, Iran. Ph.D. Thesis. Australia, University of Wollongong, unpublished, 1-412.

Mouthereau, F., Lacombe, O., Vergés, J., 2012. Building the Zagros collisional orogen: Timing, strain distribution and the dynamics of Arabia/Eurasia plate convergence. Tectonophysics, 532, 27-60.

Muller, D., Groves, D.I., Titley, S.R., 1997. Potassic igneous rocks and associated gold-cop-per mineralization. Economic Geology and the Bulletin of the Society of Economic Geologists, 92, 505.

Nakamura, Y., Tatsumoto, M., 1988. Pb, Nd, and Sr isotopic evidence for a multicomponent source for rocks of Cook-Austral islands and heterogeneities of mantle plumes. Geochimica et Cosmochimica Acta, 52, 2909-2924.

Navarro, J., Teramoto, E.H., Engelbrecht, B., Chang, H.K., 2020. Assessing hydrofacies and hydraulic properties of basaltic aquifers derived from geophysical logging. Geology, 50(4), 1-13.

Nazarinia, A., Mortazavi, M., Arvin, M., Hu, R., Zhao, C., Poosti, M., 2018. U-Pb zircon dating, Sr-Nd isotope and petrogenesis

of Sarduiyeh granitoid in SE of the UDMA, Iran: implication for the source origin and magmatic evolution. International Geology Review, 62(13-14), 1-19.

Neill, I., Meliksetian, K., Allen, M.B., Navasardyan, G., Kuiper, K., 2015. Petrogenesis of mafic collision zone magmatism: The Armenian sector of the Turkish-Iranian Plateau. Chemical Geology, 403, 24-41.

Niu, Y.L., Wilson, M., Humphreys, E.R., O'Hara, M.J., 2012. A trace element perspective on the source of ocean island basalts (OIB) and fate of subducted ocean crust (SOC) and mantle lithosphere (SML). Episodes, 35(2), 310-327.

Noorizadeh, M., Moradian, A., Ahmadipour, H., Ghassemi M.R., Santos, J.F., 2018. Petrology, Geochemistry and Tectonomagmatic Evolution of Hezar Igneous Complex (Rayen-South of Kerman- Iran): the First Description of an Arc Remnant of the Neotethyan Subduction Zone. Islamic Republic of Iran, Journal of Sciences, 29(4), 341-359.

Omrani, J., Agard, P., Whitechurch, H., Benoit, M., Prouteau, G., Jolivet, L., 2008. Arc magmatism and subduction history beneath the Zagros Mountains, Iran: A new report of adakites and geodynamic consequences. Lithos, 106, 380-398.

Orozco-Esquivel, T., Petrone, C.M., Ferrari, L., Tagami, T., Manetti, P., 2007. Geochemical and isotopic variability in lavas from the eastern Trans-Mexican Volcanic Belt: slab detachment in a subduction zone with varying dip. Lithos, 93(1), 149-174.

Özdemir, Y., Karaoğlu, Ö., Tolluoğlu, A.Ü., Güleç¸ N., 2006. Volcanostratigraphy and petrogenesis of the Nemrut stratovolcano (East Anatolian High Plateau): The most recent post-collisional volcanism in Turkey. Chemical Geology, 226, 189-211.

Pang, K.N., Chung, S.L., Zarrinkoub, M.H., Li, X.-H., Lee, H.Y., Lin, T.H., Chiu, H.Y., 2016. New age and geochemical constraints on the origin of Quaternary adakite-like lavas in the Arabia–Eurasia collision zone. Lithos, 264, 348-359.

Pearce, J.A., 1983. Role of subcontinental lithosphere in magma genesis at active continental margins: In continental basalts and mantle xenoliths. In: Hawkesworth, C.J., Norry, M.J. (eds.). Continental Basalts and Mantle Xenoliths. Nantwich, Shiva, 230-249.

Pearce, J.A., Bender, J.F., Delong, S.E., Kidd, W.S.F., Low, P.J., Guner, Y., Sargolu, F., Yilmaz, Y., Moorbath, S., Mitchell, J.G., 1990. Genesis of collision volcanism in eastern Anatolia, Turkey. Volcanology and Geothermal Research, 44, 189-229.

Pearce, J.A., 2008. Geochemical fingerprinting of oceanic basalts with applications to ophiolite classification and the search for Archean oceanic crust. Lithos, 100(1), 14-48.

Peccerillo, A., Taylor, S.R., 1976. Geochemistry of Eocene Calc-Alkaline Volcanic Rocks from the Kastamonu Area, Northern Turkey. Contributions to Mineralogy and Petrology, 58, 63-81.

Richards, J.P., 2003. Tectono-magmatic precursors for porphyry Cu–(Mo–Au) deposit formation. Economical Geology, 96, 1515-1533.

Ritter, J.R.R., Christensen, U.R., 2007. Mantle Plumes – A multidisciplinary approach. Heidelberg, Springer Verlag, 1-502.

Saadat, S., Karimpour, M.H., Stern, C., 2010. Petrochemical characteristics of Neogene and Quaternary alkali olivine basalts from the Western Margin of the Lut Block, Eastern Iran. Iranian Journal of Earth Sciences, 2, 87-106.

Saadat, S., Stern, C.R., 2012. Petrochemistry of a xenolith-bearing Neogene alkali olivine basalt from northeastern Iran. Volcanology and Geothermal Research, 225, 13-29.

Sajona, F.G., Maury, R.C., Bellon, H., Cotton, J., Defant, M.J., Pubellier, M., 1993. Initiation of subduction and the generation of slab melts in western and eastern Mindanao, Philippines. Geology, 21, 1007-1010.

Saric, A., Djordjevic, M., Dimitrijevic, M.N., 1971. Geological map of Shahr-Babak, Scale 1/100000. Tehran (Iran), Geological Survey of Iran.

Shafiei, B., Haschke, M., Shahabpour, J., 2009. Recycling of orogenic arc crust triggers porphyry Cu mineralization in Kerman Cenozoic arc rocks, southeastern Iran. Mineralium Deposita, 44, 265-283.

Shafaii Moghadam, H., Ghorbani, Gh., Zaki Khedr, M., Fazlnia, N., Chiaradia, M., Eyuboglu, Y., Santosh, M., Galindo Francisco, C., Lopez Martinez, M., Gourgaud, A., Arai, A., 2014. Late Miocene K-rich volcanism in the Eslamieh Peninsula (Saray), NW Iran: Implications for geodynamic evolution of the Turkish-Iranian High Plateau. Gondwana Research, 26(3-4), 1028-1050.

Shaker Ardakani, A., 2016. Post-collisional Plio-Pleistocene Anar-Dehaj adakitic subvolcanic domes in the central volcanic belt of Iran: geochemical characteristics and tectonic implications. Periodico di Mineralogia, 85, 185-200.

Stampfli, G.M., Borel, G.D., 2002. A Plate Tectonic Model for the Paleozoic and Mesozoic Constrained by Dynamic Plate Boundaries and Restored Synthetic Oceanic Isochrons. Earth and Planetary Science Letters, 196, 17-33.

Stocklin, J., Nabavi, M.H., 1973. Tectonic Map of Iran, 1:2,500,000. Geological Survey of Iran.

Straub, S.M., Gómez-Tuena, A., Zellmer, G.F., Espinasa-Perena, R., Stuart, F.M., Cai, Y., Langmuir, C.H., Martin del Pozzo, A.L., Mesko, G.T., 2013. The processes of melt differentiation in arc volcanic rocks: insight from OIB-type arc magmas in the central Mexican Volcanic Belt. Petrology, 54, 665-701.

Sun, S.S., Mc Donough, W.F., 1989. Chemical and isotopic systematics of oceanic basalts: implications for mantle composition and processes. In: Saunders, A.D., Norry, M.J. (eds.). Magmatism in the Ocean Basins. London, The Geological Society, 42 (Special Publications), 313-345.

Taghipour, N., Aftabi, A., Mathur, R., 2007. Geology and Re-Os Geochronology of Mineralization of the Miduk Porphyry Copper Deposit. The Society of Resource Geology, 2, 143-160.

Takin, M., 1972. Iranian geology and continental drift in the Middle East. Nature, 235, 147-150.

Tang, G.J., Wang, Q., Wyman, D.A., Li, Z.X., Zhao, Z.H., Jia, X.H., Jiang, Z.Q., 2010. Ridge subduction and crustal growth in the Central Asian Orogenic Belt: Evidence from Late Carboniferous adakites and high-Mg diorites in the western

Junggar region, northern Xinjiang (west China). Chemical Geology, 227(3-4), 281-300.

Taylor, S.R., McLennan, S.M., 1985. The Continental Crust: Its Composition and Evolution. Carlton, Blackwell Scientific Publication, 312pp.

Tunini, L., Jiménez-Munt, I., Fernàndez, M., Vergés, J., Villaseñor, A., 2015. Lithospheric mantle heterogeneities beneath the Zagros Mountains and the Iranian Plateau: a petrological-geophysical study. Geophysical Journal International, 200, 596-614.

Van Hunen, J., Allen, M.B., 2011. Continental collision and slab break-off: A comparison of 3-D numerical models with observations. Earth and Planetary Science Letters, 302, 27-37.

Verdel, C., Wernicke, B.P., Hassanzadeh, J., Guest, B., 2011. A Paleogene extensional arc flare-up in Iran. Tectonics, 30, 1-20.

Wang, Q., Wyman, D.A., Xu, J.F., Jian, P., Zhao, Z.H., Li, C.H., Xu, W., 2007. Early Cretaceous adakitic granites in the Northern Dabie Complex, central China: implications for partial melting and delamination of thickened lower crust. Geochimica et Cosmochimica Acta, 71, 2609-2636.

Wang, Q., Wyman, D., Xu, J., Wan, Y., Li, C., Zi, F., Jiang, Z., Qiu, H., Chu, Z., Zhao, Z., 2008. Triassic Nb-enriched basalts, magnesian andesites, and adakites of the Qiangtang terrane (Central Tibet): Evidence for metasomatism by slab-derived melts in the mantle wedge. Contributions to Mineralogy and Petrology, 155, 473-490.

Wang, T., Guo, L., Zhang, L., Yang, Q.D., Zhang, J.J., Tong, Y., Ye, K., 2015. Timing and evolution of Jurassic–Cretaceous granitoid magmatisms in the Mongol–Okhotsk belt and adjacent areas, NE Asia: Implications for transition from contractional crustal thickening to extensional thinning and geodynamic settings. Journal of Asian Earth Sciences, 97, 365-392.

Weaver, B.L., 1991. The origin of ocean island basalt end-member compositions: trace element and isotopic constraints. Earth and Planetary Science Letters, 104, 381-397.

Whitney, D.L., Evans, B.W., 2010. Abbreviations for Names of Rock-Forming Minerals. American Mineralogist, 95, 185-187.

Wilson, M., 1989. Igneous Petrogenesis. Springer, A global Tectonic Approach, 2, 218-222.

Winchester, J.A, Floyd, P.A., 1977. Geochemical discrimination of different magma series and their differentiation product using immobile elements. Chemical Geology, 20, 325-343.

Wilson, M., 2007. Igneous Petrogenesis. London, Chapman & Hall, 466pp.

Xiong, X., Keppler, H., Audetat, A., Ni, H., Sun, W., Li, Y., 2011. Partitioning of Nb and Ta between rutile and felsic melt and the fractionation of Nb/Ta during partial melting of hydrous metabasalt. Geochimica et Cosmochimica Acta, 75, 1673-1692.

Zarasvandi, A., Liaghat, S., Zentilli, M., Reynolds, P.H., 2007. 40Ar/39Ar geochronology of alteration and petrogenesis of porphyry copper-related granitoids in the Darreh-Zerreshk and Ali-Abad area, central Iran. Exploration and Mining Geology, 16, 11-24.

Zarasvandi, A., Shafiei, B., Pourkaseb, H., Moridi, S., 2011. Alteration and Mineralization in the Supergene zone of the Iju porphyry copper deposit, Northwestern Shahr-e-Babak, Kerman province. 2nd Symposium of Society of Economic Geology of Iran, Khoramabad, Iran.

Zarasvandi, A., Rezaei, M., Sadeghi, M., Pourkaseb, H., 2015. Rare earth element signatures of economic and sub-economic porphyry copper systems in Urumieh–Dokhtar Magmatic Arc (UDMA), Iran. Ore Geology Reviews, 70, 407-423.

Zhang, C.L., Yang, D.S., Wang, H., Takahashi, Y.C., Ye, H.M., 2011. Neoproterozoic mafic-ultramafic layered intrusion in Quruqtagh of northeastern Tarim Block, NW China: Two phases of mafic igneous activity with different mantle sources. Gondwana Research, 19, 177-190.

Zhang, G., Niu, Y., Song, S., Zhang, L., Tian, Z., Christy, A.G., Han, L., 2015. Trace element behavior and P-T-t evolution during partial melting of exhumed eclogite in the North Qaidam UHPM belt (NW China): Implications for adakite genesis. Lithos, 226, 65-80.

Zhu, D.C., Wang, Q., Chung, S.L., Cawood, P.A., Zhao, Z.D., 2018. Gangdese magmatism in southern Tibet and India-Asia convergenece since 120 Ma. In: Treloar, P.J., Searle, M.P. (eds.). Himalayan Tectonics: A Modern Synthesis. London, The Geological Society, 483 (Special Publications), 583-604.

Manuscript received October 2021;
revision accepted June 2022;
published Online August 2022.